INFORMATION TO USERS

This material was produced from a microfilm copy of the original document. While the most advanced technological means to photograph and reproduce this document have been used, the quality is heavily dependent upon the quality of the original submitted.

The following explanation of techniques is provided to help you understand markings or patterns which may appear on this reproduction.

1. The sign or "target" for pages apparently lacking from the document photographed is "Missing Page(s)". If it was possible to obtain the missing page(s) or section, they are spliced into the film along with adjacent pages. This may have necessitated cutting thru an image and duplicating adjacent pages to insure you complete continuity.

2. When an image on the film is obliterated with a large round black mark, it is an indication that the photographer suspected that the copy may have moved during exposure and thus cause a blurred image. You will find a good image of the page in the adjacent frame.

3. When a map, drawing or chart, etc., was part of the material being photographed the photographer followed a definite method in "sectioning" the material. It is customary to begin photoing at the upper left hand corner of a large sheet and to continue photoing from left to right in equal sections with a small overlap. If necessary, sectioning is continued again — beginning below the first row and continuing on until complete.

4. The majority of users indicate that the textual content is of greatest value, however, a somewhat higher quality reproduction could be made from "photographs" if essential to the understanding of the dissertation. Silver prints of "photographs" may be ordered at additional charge by writing the Order Department, giving the catalog number, title, author and specific pages you wish reproduced.

5. PLEASE NOTE: Some pages may have indistinct print. Filmed as received.

University Microfilms International
300 North Zeeb Road
Ann Arbor, Michigan 48106 USA
St. John's Road, Tyler's Green
High Wycombe, Bucks, England HP10 8HR

LASER INDUCED ATOMIC FLUORESCENCE FROM Na_2

by

JO-LIEN N. YANG

A dissertation submitted to the Graduate Faculty in Physics in partial fulfillment of the requirements for the degree of Doctor of Philosophy, The City University of New York.

1977

This manuscript has been read and accepted for the Graduate Faculty in Physics in satisfaction of the dissertation requirement for the degree of Doctor of Philosophy.

Dec. 14 1976
date

Robert Callender
Chairman of Examining Committee

Dec 15, 1976
date

Myriam P. Sarachik
Executive Officer

E. C. Ferrari

James J. Wynne

Supervisory Committee

The City University of New York

Abstract

LASER INDUCED ATOMIC FLUORESCENCE

FROM Na_2

by

Jo-Lien N. Yang

Adviser: Professor Robert H. Callender

The transient resonance between a laser beam and the electronic levels of a pair of atoms (or molecule) will produce transitions to the upper electronic state of the pair. If the kinetic energy of the pair after the transition is greater than the upper state's dissociation energy, this pair of atoms will separate and one of them will carry the excitation energy and then fluoresce in the atomic line corresponding to the atomic excited state. We have called this laser induced atomic fluorescence (LIAF). A semi-classical analysis shows that the excitation will take place at the internuclear separation at which the laser line resonates with the difference between the ground and excited electronic states. The fluorescence is then proportional to the electronic transition moment at that internuclear separation. So it is possible to map out the transition moment as a function of the nuclear separation R, by changing the laser frequency and picking out a series of R corresponding to a series of laser frequencies.

We use sodium as a sample and use both Ar^+ and Kr^+ lasers to excite Na_2 from $X^1\Sigma_g^+$ ground state to $B^1\pi_u$ excited state. By scanning the spectrometer through the D-line wavelength, we can collect the resulting D-line radiation through a photomultiplier and photon counting electronic which are interfaced with a PDP-8e computer. The spectra are stored in the PDP-8e and can be transferred to a PDP-10 computer for further analysis, e.g., calculating the D-line intensity from the observed spectra, and reducing the dissociation energy of $^1\pi_u$ state and the transition moment from the different temperature and different laser frequency data sets.

We found that the dissociation energy of the $B\ ^1\pi_u$ state is equal to $3300 \pm 200\ cm^{-1}$ and that the relative transition moment of Na_2 is constant between 2.7 and 4.1 Å.

ACKNOWLEDGEMENTS

I would like to express my deepest appreciation to my advisor, Professor Robert H. Callender, for the support and guidance he provided throughout this research. Without these this work would not be possible to finish. The constant interest and valuable suggestions for the theoretical aspects of this work from Professor Joel I. Gersten is gratefully acknowledged. I would also like to thank Dr. Richard W. Leigh for his patient, valued assistance and advice during the entire period of the experiment.

The close support from the Machine Shop of the Physics Department of the City College of New York has been invaluable. Mr. Schreiner from the Glass Shop of City University of New York deserves special recognition for his fine work with the sodium cells used in this experiment.

I also would like to express my thanks to Mr. Apostols Doukas for his interesting discussions and assistance from time to time.

Finally, and most importantly, I would like to thank Ting-Pin for his encouragement and understanding for my years of graduate work.

TABLE OF CONTENTS

LIST OF TABLES

LIST OF FIGURES

CHAPTER I

INTRODUCTION

This thesis describes a new technique called Laser Induced Atomic Fluorescence (LIAF)[1,2] and the use of this technique to measure the relative electronic transition moment of molecular systems as a function of internuclear separation. The particular case studied in detail is the molecular sodium (Na_2) system.

The Condon approximation--the neglect of the dependence of electronic transition moments on internuclear separation--is usually used to study the molecular spectra. However, the approximation is of rather limited validity for modern molecular-structure calculations. The spatial variation of the electronic transition moment must be included when analyzing absorption, emission and resonance Raman data. The experimental measurements of this variation have been scarce and have relied mainly on r-centroid technique[3] which analyzes the discrete vibrational spectra progression. This technique requires numerical calculation of the matrix element and is useful only in particular molecules and over a limited range of internuclear separation. In this thesis we develop the easier technique of LIAF to obtain directly the electronic transition moment as a function of internuclear separation.

The laser resonates with the molecule and induces a

transition from the molecular ground state to the excited state. If the energy of the excited molecule is higher than the molecular dissociation energy, the excited molecule will dissociate and produce atomic fluorescence. A semi-classical analysis shows that the excitation takes place at the internuclear separation at which laser is in resonance with the difference between the ground and excited electronic states. The transition rate, and hence the intensity of the atomic fluorescence, are then proportional to the square of the electronic transition moment at that internuclear separation. Thus by changing the laser frequency, corresponding to a series of resonant radii of r, we can map out the transition moment as a function of internuclear separation, r. This technique is what we call LIAF.

In our experiment, both Ar^+ and Kr^+ lasers were used to excite sodium molecule from ground $X\,^1\Sigma_g^+$ state to excited $B\,^1\Pi_u$ state. From these available laser frequencies, we obtain the transition moment of sodium molecule between $B\,^1\Pi_u$ and $X\,^1\Sigma_g^+$ states as function of nuclear separation, for separations between 2.7Å and 4.1Å. The analysis of this technique is very simple. It needs only the electronic potential curves. No calculation of matrix element is necessary. Moreover, this technique can be applied to both bound-bound and bound-continuum transition. As we will discuss below, LIAF can simultaneously be used to measure the dissociation energy of the excited state.

In the next chapter, we present the theory of LIAF using a semi-classical approach, the accuracy of this approach

and the derivation of the semi-classical equation of LIAF from a quantum mechanical treatment. In chapter III, the potential curves used here for Na_2 are discussed and spectroscopic parameter of these curves defined. In chapter IV, we discuss the main experimental problem, optical pumping of excited vibrational levels of the electronic ground state. Chapter V includes the experimental design, the data collection and reduction procedures and a discussion of some experimental problems. In chapter VI, we present the results of the dissociation energy of $B^1\pi_u$ state and the transition moment between $X^1\Sigma_g^+$ and $B^1\pi_u$ states, and compare them with the theory and with other available data. We calculate the scattering cross section as well. Chapter VII is our conclusion.

CHAPTER II

THEORY

A semi-classical approximation was used in the analysis of LIAF. We consider nuclear motion classically while the electronic motion is treated quantum mechanically. Since the levels of interest are closely spaced compared to kT and the excited rotation-vibrational states form a continuum, this approximation is quite reliable. In the following section, we use this approximation to derive the LIAF formula. The valid range of this approximation is determined by Wentzel-Kramers-Brillioiuin (WKB) estimation shown in section B. In section C, we show that this approximation is the first order term of a full quantum mechanical treatment.

A. Semi-classical Analysis

According to the Frank-Condon principle the relative nuclear separation, nuclear angular momentum and kinetic energy are conserved during an electronic transition. Thus we can consider the nuclear motion being frozen during the transition. Using the electric dipole approximation,[4] the Hamiltonian of the system is

$$H_t = H_o - \frac{1}{2}\mu(E_o e^{i\omega t} + E_o^* e^{-i\omega t})$$

where H_o is the unperturbed Hamiltonian for the molecular system, μ is the electric dipole operator, E_o is the electric field of the laser with frequency ω. The time dependent perturbation method was used to solve this Schrodinger equation. We obtain the transition rate, R,

$$R(r) = \left(\frac{\pi E_o^2}{2\hbar}\right) |\langle 2|\mu|1\rangle|^2 \delta(\epsilon_2(r) - \epsilon_1(r) - \hbar\omega)$$

where ϵ_1 and ϵ_2 are the instantaneous energies of the $|1\rangle$ and $|2\rangle$ states.

When the energy of the system after the induced transition is greater than the effective potential[5] of the excited state (see Fig. 1), this molecule will then separate into two atoms and emit atomic fluorescence radiation. This is the so-called LIAF. Thus the LIAF signal, $\mathcal{T}$, can be calculated by integrating the transition rate, R, over the pair distribution function, dg, with the total energy higher than effective potential,

$$\mathcal{T} = V\left(\frac{\Omega}{4\pi}\right)\int R\,\theta(E + \hbar\omega - \epsilon_2(r_o) - L^2/2mr_o^2)\,dg \qquad (1)$$

where V is the volume of the laser beam at which signal was detected, $\Omega/4\pi$ is the solid angle fraction subtended by the detector, E is the molecular energy before transition is induced, r_o is the location of the peak of the effective potential barrier and L is the angular momentum. θ is the step function with value 1 for positive argument, and 0 for negative argument. Only the former case, which corresponds to a system

Figure 1

Energy levels of Na_2 used in these experiments, assuming $L = 0$, with various parameters of the levels shown. A transition in a molecule having just enough initial energy to permit photodissociation, and hence atomic fluorescence, is shown; r_e refers to the molecular equilibrium internuclear separation.

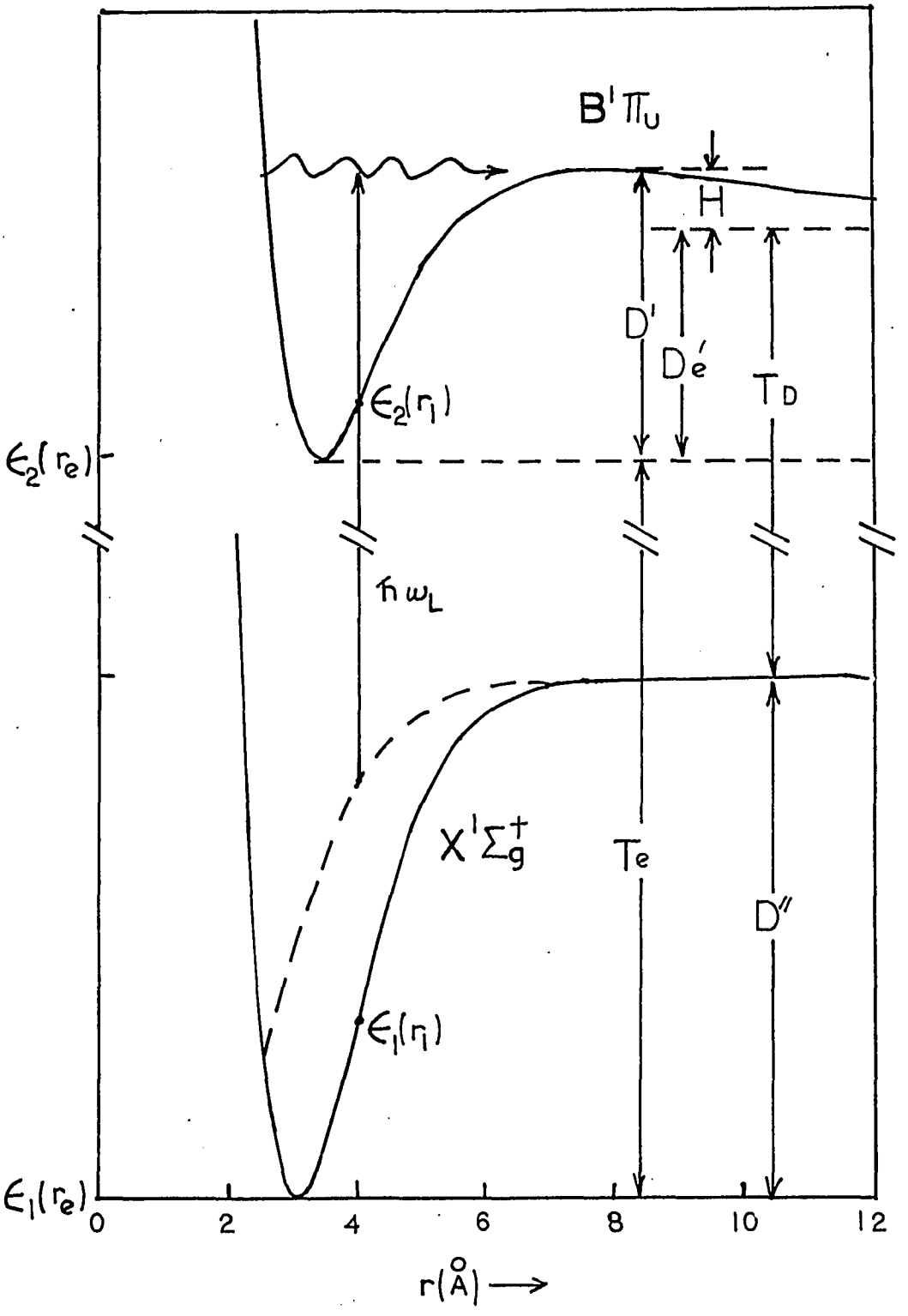
B¹Πu
H
D'
D'e
TD
ε2(re)
ε2(r1)
ħωL
X¹Σg+
Te
D''
ε1(r1)
ε1(re)
0
2
4
6
8
10
12
r(Å) ⟶

energy, $E + \hbar\omega$, higher than the effective potential, $\epsilon_2(r_o) + L^2/2mr_o^2$, contribute the LIAF signal. The pair distribution function, dg, is

$$dg = N e^{-\beta E} \cdot \sin\theta \cdot r^2 \, dr \, d\theta \, d\varphi \, dP_r \, dP_\theta \, dP_\varphi \tag{2}$$

E, L^2 are given by

$$E = \epsilon_1(r) + \frac{1}{2m}\left(P_r^2 + L^2/r^2\right)$$

$$L^2 = P_\theta^2 + P_\varphi^2/\sin^2\theta$$

and N, the normalization factor, is defined by the relation

$$\int dg \equiv \frac{n^2}{2} \int e^{-\beta\epsilon_1(r)} \, d\tau$$

with n being atomic density, the spatial volume element $d\tau = r^2 \sin\theta \, dr \, d\theta \, d\varphi$.

We found that N is equal to $(n^2/2)(\beta/2\pi m)^{3/2}$, by integrating

$$\int dg = N \int_0^\infty r^2 dr \int_0^\pi d\theta \int_0^{2\pi} d\varphi \iiint_{-\infty}^{\infty} dP_r \, dP_\theta \, dP_\varphi$$

$$\cdot e^{-\beta\left(\epsilon_1(r) + \frac{1}{2m}\left(P_r^2 + P_\theta^2/r^2 + P_\varphi^2/r^2\sin^2\theta\right)\right)}$$

$$= N \left(\frac{2\pi m}{\beta}\right)^{3/2} \int e^{-\beta\epsilon_1(r)} \, d\tau$$

$$\equiv \frac{1}{2} n^2 \int e^{-\beta\epsilon_1(r)} \, d\tau$$

Combining equations (1) and (2), we obtain the fluorescence signal

$$\Gamma = V\left(\frac{\Omega}{4\pi}\right)\int R\,\theta\left(E+\hbar\omega-\epsilon_2(r_o)-L^2/2m r_o^2\right) \cdot N e^{-\beta E}\, r^2\, dr\, d\theta\, d\varphi\, dP_r\, dP_\theta\, dP_\varphi \tag{3}$$

Since the integrand is function of r, E and L^2, the integration may be simplified by changing variable $dP_r dP_\theta$ to dEdL

$$dP_r = \frac{m\, dE}{\sqrt{2m(E-\epsilon_1(r)-L^2/r^2}}$$

$$dP_\theta = \frac{L\, dL}{\sqrt{L^2 - P_\varphi^2/\sin^2\theta}}$$

Thus Γ becomes

$$\Gamma = V\left(\frac{\Omega}{4\pi}\right)\int R\,\theta\left(E+\hbar\omega-\epsilon_2(r_o)-L^2/2m r_o^2\right) \cdot N e^{-\beta E}\,\frac{m}{\sqrt{2m(E-\epsilon_1(r)-L^2/r^2)}} \cdot \frac{L}{\sqrt{L^2-P_\varphi^2/\sin^2\theta}}\, r^2\, dr\, d\theta\, d\varphi\, dE\, dL\, dP_\varphi$$

$$= V\left(\frac{\Omega}{4\pi}\right)\int_0^\infty L\,dL\int_0^\infty r^2 dr\int_0^\infty dE\;\frac{16\pi^2 m}{\sqrt{2m(E-\epsilon_1(r)-L^2/r^2)}} \cdot N e^{-\beta E}\, R(r)\,\theta\left(E+\hbar\omega-\epsilon_2(r_o)-L^2/2m r_o^2\right)$$

After integrating over E and r, Γ is found to be,

$$\Gamma = V\left(\frac{\Omega}{4\pi}\right)\frac{n^2\pi^2 E_o^2}{\hbar}\,\frac{|\langle 2|\mu|1\rangle|^2}{|d(\epsilon_2(r)-\epsilon_1(r))/dr|} \cdot e^{-\beta\epsilon_1(r)}\, r^2\, G(r)\Big|_{r=r_i} \tag{4}$$

where r_1 is the nuclear separation of resonance; also

$$\hbar\omega = \epsilon_2(r_1) - \epsilon_1(r_1)$$

and

$$G(r_1) = (\beta/m r_1^2) \int_0^\infty dL\, L\, \mathrm{erfc}(U_L)\, e^{-\beta L^2/2m r_1^2} \tag{5}$$

with the error function[6] given by

$$\mathrm{erfc}(U_L) = \frac{2}{\sqrt{\pi}} \int_{U_L}^\infty e^{-t^2}\, dt$$

and

$$U_L = \left\{ \beta\left(\epsilon_2(r_0) - \epsilon_2(r_1) + \frac{L^2}{2m r_0^2} - \frac{L^2}{2m r_1^2}\right) \right\}^{1/2}$$

or 0 depending on whether the argument of the square root is positive or negative respectively.

Equation (4) shows that the atomic fluroescence signal, $\mathcal{P}$, is proportional to the square of the electronic transition moment at the internuclear separation, r_1, with the laser in resonance with the difference between the ground- and excited-electronic state, $|1\rangle$ and $|2\rangle$ respectively. The factor G is the correction for the metastable[7] or bound excited dimers with insufficient initial kinetic energy to photodissociate after absorbing a photon.

G, expressed by equation (5), is for general case where the excited state is bound and with a real bump or with an effective potential bump from the rotational part. This is

the case of B $^1\pi_u$ state of a sodium molecule.[8] For the case in which the excited state has no effective potential barrier, the molecule with energy higher than the asymptotic limit of the excited state will dissociate after being excited. So we can modify equation (5) by replacing r_o, the location of the peak of the effective potential, by infinity to get a simpler form of the correction factor, G'

$$G' = \lim_{r_o \to \infty} \frac{\beta}{m r_i^2} \int_0^\infty L\, dL\, \mathrm{erfc}(U_L)\, e^{-\beta L^2/2 m r_i^2} \tag{6}$$

In the above formula, only U_L depends on r_o. We define

$$U_L' = \lim_{r_o \to \infty} U_L$$

$$= \lim_{r_o \to \infty} \left\{ \beta \left(\epsilon_2(r_o) - \epsilon_2(r_i) + L^2/2 m r_o^2 - L^2/2 m r_i^2 \right) \right\}^{1/2}$$

$$= \begin{cases} \left[\beta \left(\epsilon_2(\infty) - \epsilon_2(r_i) - L^2/2 m r_i^2 \right) \right]^{1/2} \\ 0 \end{cases}$$

Equation (6) is then rewritten as

$$G' = \frac{\beta}{m r_i^2} \int_0^\infty L\, dL\, \mathrm{erfc}(U_L')\, e^{-\beta L^2/2 m r_i^2}$$

$$= \mathrm{erfc}(t) + \frac{2}{\sqrt{\pi}}\, t\, e^{-t^2}$$

where $t = \sqrt{\beta \left(\epsilon_2(\infty) - \epsilon_2(r_i) \right)}$

or 0 depending on the argument of the square root is positive

or negative. The latter case is for the unbound excited state, the correction factor, G' = erfc(0), being equal to 1. In this case, after the transition to the excited state is induced, all the atomic pairs will dissociate and emit atomic fluorescence radiation. So the LIAF signal for unbound excited states[9], Γ , is further simplified to

$$\Gamma = V\left(\frac{\Omega}{4\pi}\right) \frac{n^2\pi^2 E_0^2}{\hbar} \frac{|\langle 2|\mu|1\rangle|^2}{\left|\frac{d(\epsilon_2(r_1) - \epsilon_1(r_1))}{dr}\right|} r_1^2 \, e^{-\beta\epsilon_1(r_1)}$$

B. Estimation of the Semi-classical Approximation

A semi-classical approximation is used to derive the LIAF formula shown above. We now use the WKB method[10] to estimate the error of treating nuclear motion classically. According to WKB method, quantum mechanical effects can be neglected if the WKB parameter, W,

$$W = M\hbar \left|\frac{dU}{dr}\right| / P^3 \qquad (7)$$

is much smaller than 1, where P is linear momentum, M is reduced mass and U is effective potential. P and U are given by

$$P = \sqrt{2M(E - U)}$$

and $$U = \epsilon(r) + L^2/2Mr^2$$

where E is total energy and L is the angular momentum.

In our particular case in order to emit LIAF signal,

the energy of the excited state must be greater than or equal to the effective dissociation energy of the excited state,

$$E_m = \epsilon_2(r_0) + L^2/2M r_0^2 \quad .$$

Thus the minimum linear momentum of the atoms which will dissociate, is

$$P_m(r, L) = \sqrt{2M(E_m - \epsilon_2(r) - L^2/2M r^2)}$$

The corresponding energy of the ground state is

$$E(r,L) = E_m - \hbar\omega = E_m - (\epsilon_2(r) - \epsilon_1(r))$$

with linear momentum P,

$$P = \sqrt{2M(E - \epsilon_1(r) - L^2/2M r^2)} \quad ,$$

which is just the momentum of the excited state. From equation (7), it is clear that the WKB parameter becomes smaller as the momentum P becomes greater than P_m. Therefore, P_m can be used to calculate the maximum value of WKB parameter, W(r,L), to estimate the error in the semiclassical approach. With Equation (7) and U one has,

$$W(r,L) = \frac{M\hbar \left|\frac{dU}{dr}\right|}{P_m^3} = \frac{M\hbar \left|\frac{d}{dr}(\epsilon_2(r) + L^2/2M r^2)\right|}{(2M(E_m - \epsilon_2(r) - L^2/2M r^2))^{3/2}}$$

$$= \frac{\hbar}{2\sqrt{2M}} \frac{|d\epsilon_2(r)/dr - L^2/M r^3|}{(\epsilon_2(r_0) + L^2/2M r_0^2 - \epsilon_2(r) - L^2/2M r^2)^{3/2}}$$

where the angular momentum, L, is equal to $\hbar J$. We then average $W(r,\hbar J)$ over a Boltzman distribution of the rotational states including the rotational degeneracies,

$$W(r) = \phi \int_0^\infty (2J+1)\, e^{-\phi J(J+1)}\, W(r,\hbar J)\, dJ \qquad (8)$$

where $\phi = hc\, B_e''$, B_e'' being the first order rotational constant. The results of the numerical calculation of equation (8) at T=275°C are shown in Table 1. This table also includes the radii of resonance and the accurate wave-number[11] corresponding to various Ar^+ and Kr^+ laser lines used in this experiment. This table shows that all laser lines (except 4545 Å and 4579 Å of the Ar^+ laser) give a WKB parameter much smaller than our experimental errors. Therefore the quantum mechanical effect can be neglected for all except these two lines. We have omitted these two lines in our data analysis.

C. Derivation of the Classical Result from Quantum Mechanics

The semi-classical approximation, used and discussed above, can be derived from a standard quantum mechanical expression for the transition probability as the first term in an expansion in the commutators of the relevant operators.[12]

By the first order Born-Oppenheimer approximation, the LIAF signal can be obtained by using the Fermi-Golden rule summing over final states with final energy greater than the dissociation energy and averaging over all initial states,

TABLE 1

The wavelength ($\mathring{A}$) and frequencies (cm^{-1}) of the argon and krypton laser lines used in this study. Corresponding to each line is the internuclear distance, r ($\mathring{A}$), at which the laser frequency is resonant with the energy difference of the $^1\Sigma_g^+$ and $^1\pi_u$ states, and the WKB parameter, W(r), which determines the accuracy of the semi-classical approximation used here.

TABLE 1

λ(Å)	$\bar{\nu}_L$(cm^{-1})	r(Å)	W(r)
4545 (Ar)	21995.9	2.563	25.4
4579 (Ar)	21831.1	2.624	9.41
4658 (Ar)	21463.0	2.770	.221
4727 (Ar)	21149.8	2.892	.046
4762 (Kr)	20991.9	2.954	.029
4765 (Ar)	20981.2	2.959	.029
4825 (Kr)	20718.9	3.065	.020
4846 (Kr)	20627.3	3.103	.012
4880 (Ar)	20486.7	3.162	.009
4965 (Ar)	20135.1	3.317	.003
5017 (Ar)	19926.1	3.415	.0002
5145 (Ar)	19429.8	3.674	.004
5208 (Kr)	19194.8	3.815	.006
5287 (Ar)	18909.4	4.010	.009
5309 (Kr)	18832.0	4.069	.010

$$P = \frac{n^2 V}{2Z} \frac{\Omega}{4\pi} \sum_I e^{-\beta \epsilon_I} \sum_F \frac{\pi^2 E_0^2}{h} |\langle I|\mu(r)|F\rangle|^2$$

$$\cdot \delta(\epsilon_F - \epsilon_I - h\omega)\, \theta(\epsilon_F - D_J) \qquad (9)$$

where $|I\rangle$, the initial state with energy ϵ_i, and $|F\rangle$, the final state with energy ϵ_F, are the rotational-vibrational levels of ground and excited state, respectively, and $\mu(r)$ is the electronic transition moment depending on nuclear separation r. The partition function, Z, is

$$Z = \sum_I e^{-\beta \epsilon_I}$$

The dissociation energy, D_J, is given by

$$D_J = \left\{ \epsilon_2(r) + J(J+1)\hbar^2/2Mr^2 \right\}_{max}$$

For simplicity, we drop the $\Delta J = \pm 1$ transitions and consider only Q transition (i.e., the $\Delta J = 0$ transition); the only inaccuracy is a slight misrepresentation of the very small number of transitions for which $\Delta J = +1$ transition might dissociate, for instance, while the $\Delta J = 0$ and -1 would not. Equation (9) includes all $(n^2V/2)$ pairs in the volume V with atomic number density n.

The integral representations[13] of $\delta(x)$ and $\theta(x)$ are

$$\delta(x) = \int_{-\infty}^{\infty} \frac{e^{-ixt}}{2\pi}\, dt$$

and

$$\theta(x) = \int_{-\infty}^{\infty} \frac{e^{ikx}}{2\pi i k}\, dk \qquad (10)$$

Substituting equation (10) into (9), we have

$$P = \frac{n^2 V}{8 z} \frac{\pi E_0^2 \Omega}{h} \sum_I \sum_F e^{-\beta \epsilon_I} |\langle I| \mu(r) |F\rangle|^2$$
$$\cdot \int_{-\infty}^{\infty} dt \frac{e^{-i(\epsilon_F - \epsilon_I - h\omega)t}}{2\pi} \int_{-\infty}^{\infty} dk \frac{e^{ik(\epsilon_I + h\omega - D_J)}}{2\pi i k}$$

$$= \frac{n^2 V}{8 z} \frac{\pi E_0^2 \Omega}{h} \int_{-\infty}^{\infty} dt \frac{e^{ih\omega t}}{2\pi} \int_{-\infty}^{\infty} dk \frac{e^{ikh\omega}}{2\pi i k} S_I \qquad (11)$$

where

$$S_I = \sum_I e^{-\beta \epsilon_I} e^{i(k+t)\epsilon_I} e^{-ikD_J} \sum_F |\langle I| \mu(r) |F\rangle|^2 e^{-i\epsilon_F t}$$

ϵ_I is the eigenvalue of the ground state system with eigen function $|I\rangle$, i.e.

$$H_t |I\rangle = (T + \epsilon_1(r)) |I\rangle$$
$$= \epsilon_I |I\rangle$$

where T is the kinetic energy operator, $P^2/2m$. Similarly, for the excited state, one has

$$H_t |F\rangle = (T + \epsilon_2(r)) |F\rangle$$
$$= \epsilon_F |F\rangle$$

Using these relations, S_I can be written as

$$S_I = \sum_I e^{-ikD_J} \sum_F e^{-(\beta - ik)\epsilon_I} \langle I|\mu^+|F\rangle\langle F|\mu|I\rangle \cdot e^{it\epsilon_I} e^{-it\epsilon_F}$$

$$= \sum_I e^{-ikD_J} \langle I| e^{-(\beta-ik)(T+\epsilon_1)} \mu^+ \sum_F |F\rangle\langle F| \cdot e^{-i(T+\epsilon_2)t} \mu e^{i(T+\epsilon_1)t} |I\rangle$$

$$= \sum_I e^{-ikD_J} \langle I| e^{-(T+\epsilon_1)(\beta-ik)} \mu^+ e^{-i(T+\epsilon_2)t} \cdot \mu e^{i(T+\epsilon_1)t} |I\rangle$$

where we use the closure relation on the final states,

$$\sum_F |F\rangle\langle F| = 1$$

The operator expansions,[14] such as $e^{a+b} = e^a e^b (1-[a,b]/2+....)$ and $be^a = e^a b - e^a[a,b]+...$, are applied to expand S_I. With the second and the higher order commutators dropped, we have,

$$S_I = \sum_I e^{-ikD_J} \langle I| e^{-(\beta-ik)T} e^{-(\beta-ik)\epsilon_1} \cdot (1 + (\beta-ik)^2 [T,\epsilon_1]/2) \mu^+ e^{-iTt} \cdot e^{-i\epsilon_2 t} (1 + t^2 [T,\epsilon_2]/2) \mu e^{iTt} \cdot e^{i\epsilon_1 t} (1 + t^2 [T,\epsilon_1]/2) |I\rangle$$

The commutator of T and the r-dependent function is the derivative of this function $[T,f(r)] = -\frac{i\hbar P}{m}\frac{df(r)}{dr}$. With the

assumption that the derivative of the transition moment and the potential function are small we drop all the commutators. S_I is then simplified as

$$S_I = \sum_I e^{-ikD_J} \langle I | e^{-(\beta - ik)T} e^{-(\beta - ik)\epsilon_1} \mu^+ \mu \cdot e^{-itT} e^{-i\epsilon_2 t} e^{-itT} e^{itT} | I \rangle$$

$$= \sum_I e^{-ikD_J} \langle I | e^{-(\beta - ik)T} e^{-(\beta - ik)\epsilon_1} \mu^+ \mu \cdot e^{-i(\epsilon_2 - \epsilon_1)t} | I \rangle$$

where e^{iTt} and e^{-iTt} cancel each other according to the classical Frank-Condon principle (the kinetic energy is conserved during an electronic transition). We then decompose the last expression by a basis set of eigen-vectors of position and linear momentum,

$$\int \frac{d^3p\, d^3r}{h^3} | p \rangle \langle p | r \rangle \langle r |$$

$$S_I = \sum_I e^{-ikD_J} \int \frac{d^3r\, d^3p}{h^3} \langle I | e^{-(\beta - ik)P^2/2m} | p \rangle \cdot \langle p | r \rangle \langle r | e^{-(\beta - ik)\epsilon_1} \mu^+ \mu e^{-i(\epsilon_2 - \epsilon_1)t} | I \rangle$$

Further use of the relation

$$\sum_I \langle I | p \rangle \langle p | r \rangle \langle r | I \rangle = 1$$

leads to

$$S_I = \int \frac{d^3r\, d^3p}{h^3}\; e^{-(\beta - iK)p^2/2m}\, e^{-(\beta - iK)\epsilon_1}\, |\mu|^2 \cdot e^{-i(\epsilon_2 - \epsilon_1)t}\, e^{-iKD_J}$$

Substituting this expression back into equation (11), we obtain

$$\Gamma = \frac{n^2 V}{8\pi} \frac{\pi E_0^2 \Omega}{h} \int \frac{d^3p\, d^3r}{h^3}\, \mu^2(r)\, e^{-\beta(\epsilon_1 + p^2/2m)} \cdot \delta(\hbar\omega + \epsilon_1 - \epsilon_2)\, \theta\left(\hbar\omega + \frac{p^2}{2m} + \epsilon_1 - D_J\right) \tag{12}$$

By the same procedure, the partition function, Z, can be evaluated as

$$Z = \sum_I e^{-\beta\epsilon_I} = \int \frac{d^3p\, d^3r}{h^3}\; e^{-\beta\left(\frac{p^2}{2m} + \epsilon_1(r)\right)} \tag{13}$$

Both of these equations, (12) and (13), are identical to equations (3) and (2) which we already discussed within the context of semiclassical approximation. Thus, the semi-classical approach we employed is fully justified.

CHAPTER III

POTENTIAL CURVES

The potential curves that have been used in this work are based on Rydberg-Klein-Rees (RKR) potentials constructed from molecular spectroscopic data[18,19]. For the ground state, $^1\Sigma_g^+$, the RKR potential covers the range of the resonance radii. Aitken's method[15] is used for interpolation of the intermediate value of r. Similarly, this applies to the first excited state, $^1\pi_u$, except the 4545 Å Ar^+ laser line which resonates at a radius smaller than that given by RKR potential. Since this line is not included in our experiment, the method of extrapolation is not important in the range of shorter internuclear separation.

At larger internuclear separation near the dissociation energy, spectroscopic data is hard to obtain. For the ground state the extrapolation is unimportant. But for the excited state if the potential hill exists, (see Fig. 1), the LIAF signal then depends on the potential curve at a large nuclear separation. By choosing a suitable extrapolation function with adjusting parameters and proper analysis of the LIAF signal, we can find the height of the potential barrier which depends on the adjusting parameter in the potential function described below.

At large nuclear separation the overlap of the charge

distributions between two atoms (of the diatomic molecule) is small so the instantaneous interaction energy,[16] V_I, between the two atoms can be expanded into power series of (1/r) where r is the internuclear separation. More explicitly,

$$V_I(r) = \frac{q_1 q_2}{r} + \frac{q_2(\vec{\mu}_1 \cdot \hat{r}) - q_1(\vec{\mu}_2 \cdot \hat{r})}{r^2} + \frac{q_1 Q_2 + q_2 Q_1}{r^3}$$

$$+ \frac{\vec{\mu}_1 \cdot \vec{\mu}_2 - 3(\vec{\mu}_1 \cdot \hat{r})(\vec{\mu}_2 \cdot \hat{r})}{r^3} + \cdots\cdots\cdots$$

where q_1, q_2 are total charges of the first and second atom respectively. μ_1, μ_2 are the respective dipole moments, Q_1, Q_2 are the quadrupole moments for each charge distribution. For neutral atoms, q_1 and q_2 are zero. Thus the instantaneous interaction energy is

$$V_I(r) = \frac{a_1}{r^3} + \frac{a_2}{r^4} + \frac{a_3}{r^5} + \cdots\cdots$$

where $$a_1 = \vec{\mu}_1 \cdot \vec{\mu}_2 - 3(\vec{\mu}_1 \cdot \hat{r})(\vec{\mu}_2 \cdot \hat{r})$$

The first term corresponds to the dipole-dipole interaction, the second term to the dipole-quadrupole interaction, the third term to the quadrupole-quadrupole interaction, etc. According to standard theory, the first order perturbation energy[17] is

$$\Delta E = \langle \Psi | V_I | \Psi \rangle$$

where Ψ is the molecular electronic wave function for the

system. For the $^1\pi_u$ state,

$$|\psi\rangle = \frac{1}{\sqrt{2}} \left(|3S, 3P_1\rangle + |3P_1, 3S\rangle \right)$$

The contributions from dipole-quadrupole interaction and quadrupole-quadrupole interaction are all zero because of parity and symmetry arguments. Thus, the first order energy term is proportional to $1/r^3$ or,

$$\Delta E = \frac{p^2}{r^3} \tag{14}$$

where p is one component of the electric dipole moment for the $3\,^2P$-$3\,^2S$ atomic transition in sodium. The second order perturbation energy for this $^1\pi_u$ state gives $1/r^6$ and $1/r^8$ dependence by the same consideration of symmetry. Thus for the $^1\pi_u$ excited state, the dipole-dipole interaction potential is repulsive as is easily seen from equation (14): it overcomes the higher order terms of the electrostatic interaction and exchange force which produces the stable well. As shown in Figure 1 there is potential hill on the excited ($^1\pi_u$) state, but not on the ground state, since first order perturbation for the dipole-dipole interaction vanishes for the ground state.

There exists several reports about this potential hill. King and Van Vleck[8] estimated the height of this bump to be 800 cm^{-1}. Hessel and Kusch[18] made an estimate of 485 cm^{-1} based on the spectroscopic work. Demtroder and Stock[19]

published a value of 550 ± 120 cm^{-1} above the $(3^2P_{1/2}, 3^2S_{1/2})$ state of the separated atoms, or 560 ± 120 cm^{-1} above $(3^2P_{1/2}, 3^2S_{1/2})$ state if the fine structure is taken into account.

The intensity of LIAF signal is sensitive to the dissociation energy of the excited state, D' (see Fig. 1), through G(r) and U_L (equation (5)). However, equation (5) shows that G(r) depends on the maximum value of the effective potential, $V_{eff} = \epsilon_2(r_o) + L^2/2mr_o^2$. We also note that the maximum value of V_{eff} and the corresponding r_o change with angular momentum L. So the functional form of the excited potential $\epsilon_2(r)$ to find r_o and $(V_{eff})_{max}$ is needed for the value of r which the RKR method does not cover. Since the exchange force is quite small for sodium beyond 5 Å,[21] we chose an asymtotic potential based on an electrostatic expansion

$$\epsilon_2(r) = T_e + D_e' + p^2/r^3 - c/r^6 - d/r^8 \qquad (15)$$

Here p is the electric dipole moment of 3^2P-3^2S atomic transition as discussed before, c and d are calculated to fit the last two RKR points to make this curve join smoothly. When the experimental value of (p^2),[22] $2.04*10^5$ cm^{-1}-Å^3, was used in equation (15), this expression did not give the dissociation energy within expected range of 3000-3300 cm^{-1}. A value of p^2 about two to three times that value is needed to give a proper dissociation energy. We thus consider p^2 as an adjustable parameter. This failure of equation (15) to adequately describe physical situation, may be due to the fact

that the overlap and exchange effect are not negligible. In order to test if our results depend on different potential model, we fitted the same data set with the values of D_e'=150 cm^{-1} greater and less than Hessel's value which we used for analysis and with potentials of the form

$$\epsilon_2(r) = T_e + D_e' + P^2/r^3 - C/r^4 - D/r^5$$

and

$$\epsilon_2(r) = T_e + P^2/r^3 + D_e'(1 - e^{-(r-r_0)\alpha})$$

which produced variations in the location of the maximum of the L=0 potential from 7.2 Å to 7.7 Å. In all of these cases, the variation in the result of dissociation energy D' was only a few wavenumber which is much less than the statistical uncertainty associated with the measurement.

Since the energy difference between the bottom of the potential well of the ground state and that of the excited state, T_e, and the energy of D-line, T_D, are known very accurately (T_e = 20319.2 cm^{-1}, T_D = 16960.85 cm^{-1} (Ref. 20)), an estimate of the height of the bump, H, can be obtained through the relation

$$H = T_e + D' - T_D - D''$$

where D" is dissociation energy of the ground state. However, the values of D" as measured separately by Demtroder[19] and Hessel[18] are different by 100 cm^{-1}. Due to this disagreement,

the precise height of the bump remains uncertain for the time being. So the comparison of H is somewhat inconclusive, and beginning in Chapter V we compare the dissociation energy, D', instead of H.

CHAPTER IV

OPTICAL PUMPING EFFECT

In the preliminary experiment, we found that for temperatures above 350°C D-line radiation was also enhanced by some effects not described by equation (4). In order to examine these effects, we measured the variation of the LIAF signal as a function of the single mode laser frequencies (high resolution LIAF experiment) as described in Section A. In Section B, we discussed some possible effects to explain this enhancement.

A. High Resolution LIAF Experiment

1. Heat Pipe

Sodium is a very active element. It reacts with almost any material, especially at high temperature, giving a colored product. Making a transparent sodium vapor's container is rather difficult. For temperature higher than 300°C, we used a heat pipe oven system. This heat pipe oven[27] is shown in Fig. 2. It consists of a tube with a capillary structure on the inner surface, heater around the center of the outside tube, and windows on both ends.

The main tube was made of 347 stainless steel; 1.9 cm o.d., 1.6 cm i.d. and 30 cm long. The wick, made of 100-mesh 304 stainless steel screen with 0.13 mm diameter wires,

Figure 2

Diagrammatic Sketch of the Heat Pipe Oven

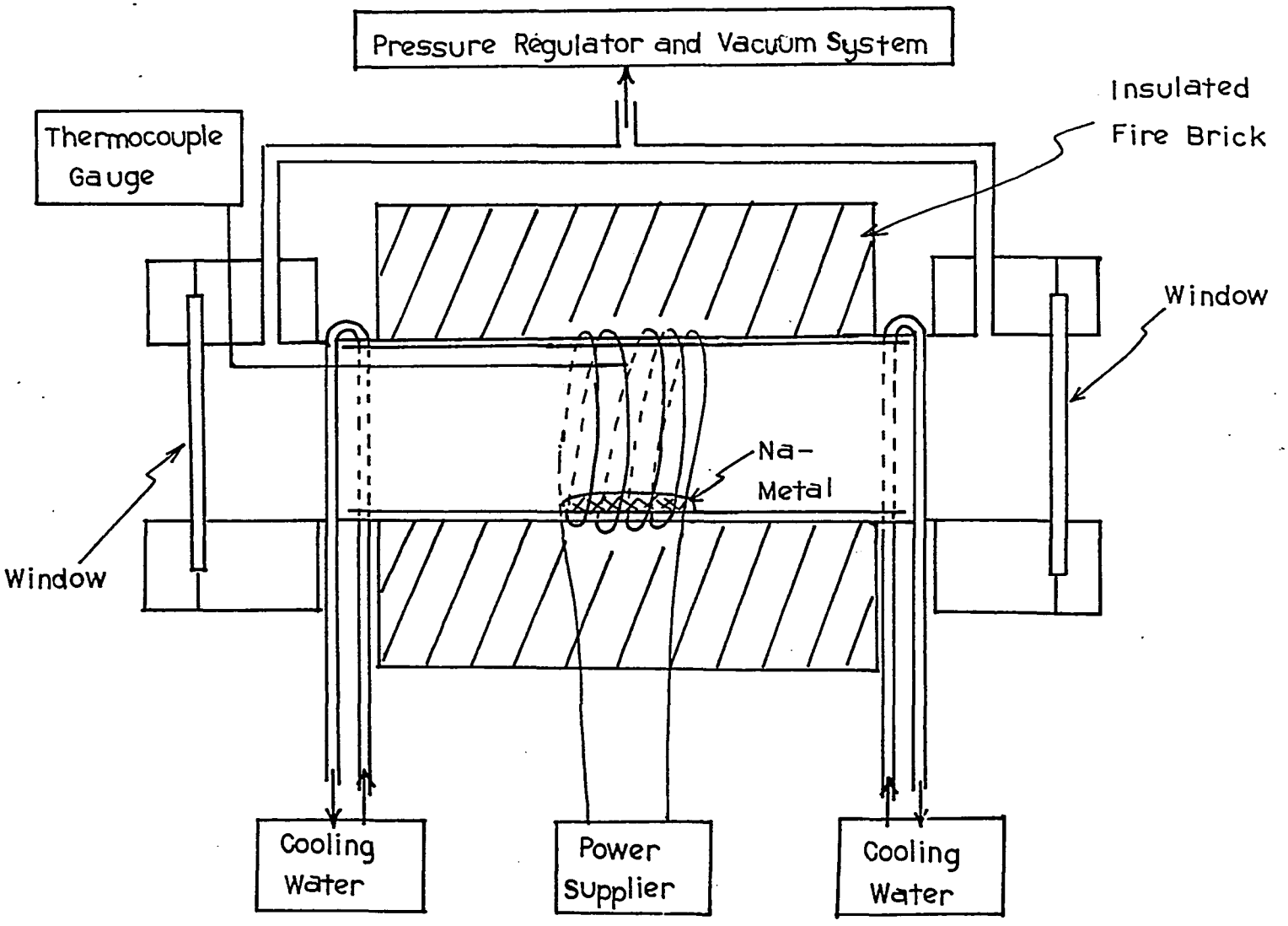
Pressure Regulator and Vacuum System
Thermocouple Gauge
Insulated Fire Brick
Window
Window
Na-Metal
Cooling Water
Power Supplier
Cooling Water

completely covered the inner tube with about three to four folds. The copper tube, passing through the cooling water, was mounted on both ends of the tube to keep the windows cool.

Insulated fire bricks were used to surround the heater and most of the tube. The whole system was connected to a vacuum station and buffer gas container with a pressure regulator[28] to control the buffer gas pressure. Ar gas was used as the buffer gas and it was kept between window and the vapor zone (as explained below), which removed the problem of contaminating the window.

The operation of the heat pipe starts at heating the center of the tube to melt the sodium metal. The melted sodium metal wets the wick and continuously produces the sodium vapor. This vapor then diffuses to both ends of the tube till it meets the cool Ar gas and condenses. The condensate through the wick returns back to the center by capillary action. Due to this action of the sodium flow, the sodium vapor is self-purified and is completely separated from the Ar gas except for a short transition region. When the system reaches equilibrium, the central part of the heat pipe is full of sodium vapor at a temperature corresponding to the sodium vapor pressure[29] which is equal to or just exceeds the buffer gas pressure. So by adjusting the Ar gas pressure, the sodium vapor temperature, which was also measured by the chromel-alumel thermocouple mounted inside the tube for double check, can be controlled.

2. Optical Setup

The experimental setup is shown in Fig. 3. Laser light was focused into the sodium vapor. The resulting LIAF signal was detected in a backscatter geometry and focused into a Spex double monochrometer equipped with a cooled photomultiplier and photon-counting electronics.

The spectrometer was set at one of the D-line wavenumber (16960 cm^{-1}). The Ar^+ laser was operated in a single mode by a quartz etalon in a temperature controlled oven. When the oven was turned off, the single mode would sweep slowly across the laser beam profile. We recorded the LIAF signal during the time that single mode was moving in one cycle. At the same time, the laser intensity after passing through the heat pipe was plotted. The laser was kept in light mode control, so that the laser power output was constant within ±3% over the whole cycle.

3. Results on the High Resolution LIAF Experiment

Typical results of the dependence of the D-line intensity as a function of single mode laser frequency are shown in Fig. 4. At higher temperature the data show peaks at some particular laser frequencies. These peaks coincided with the location of the maximum absorption in the transmission data, corresponding to the particular molecular resonances. As the temperature was lowered, the structure weakened and then disappeared for all the laser lines except the 5017 Å Ar line retained a noticeable peak at the high frequency edge of the laser gain profile at all temperatures. We have thus neglected this line from our results. For

Figure 3

Preliminary LIAF Experimental Arrangement

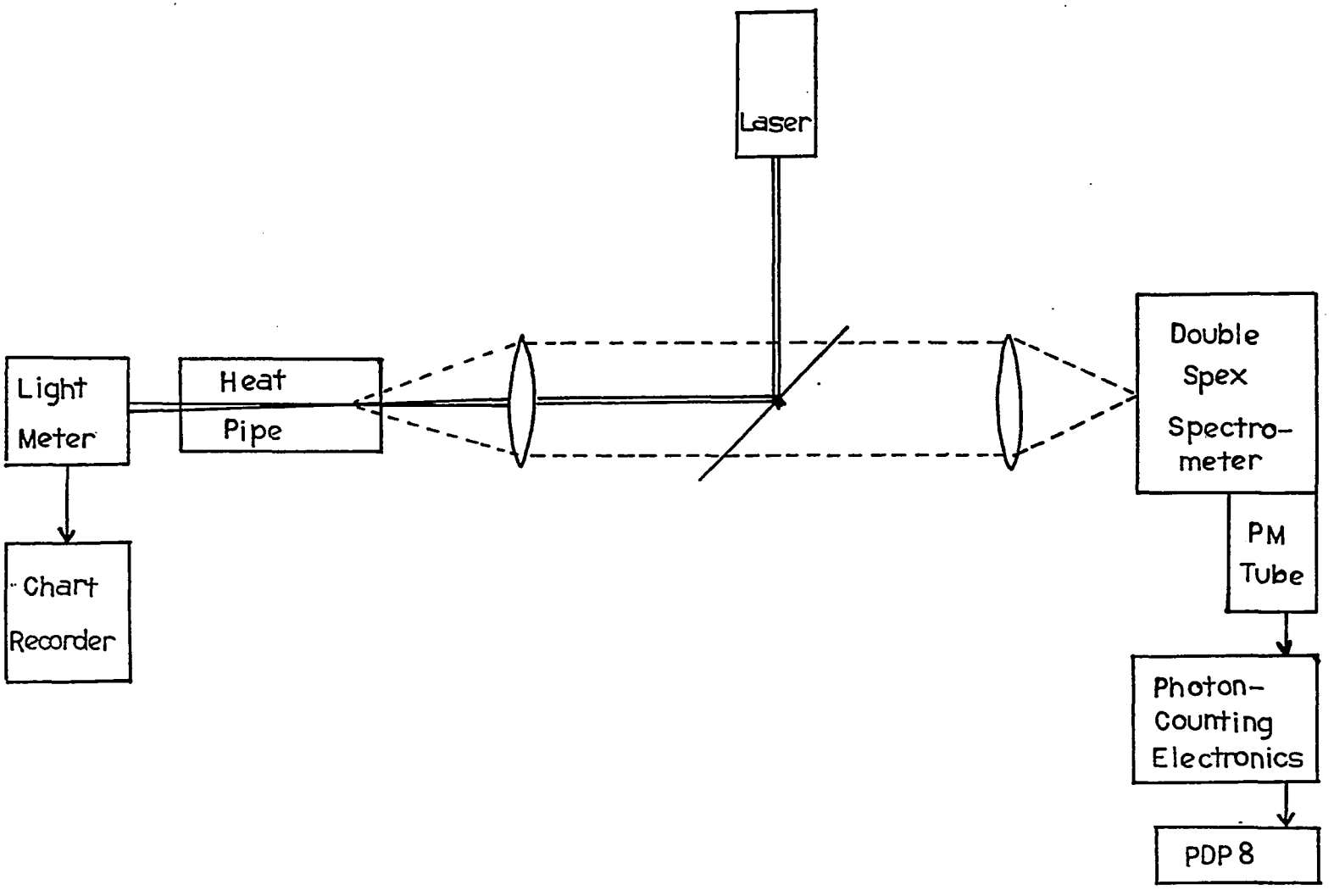
Laser
Light Meter
Heat Pipe
Double Spex Spectro-meter
PM Tube
Chart Recorder
Photon-Counting Electronics
PDP 8

Figure 4

The resultant high resolution LIAF signal showing the effects of optical pumping at high pressures, as a function of laser frequency from one end of the gain profile of the 4880 Å laser line to the other. In (a) the gas pressure is low corresponding to a temperature of 300°C; in (b) the gas pressure is greater with a cell temperature of 350°C.

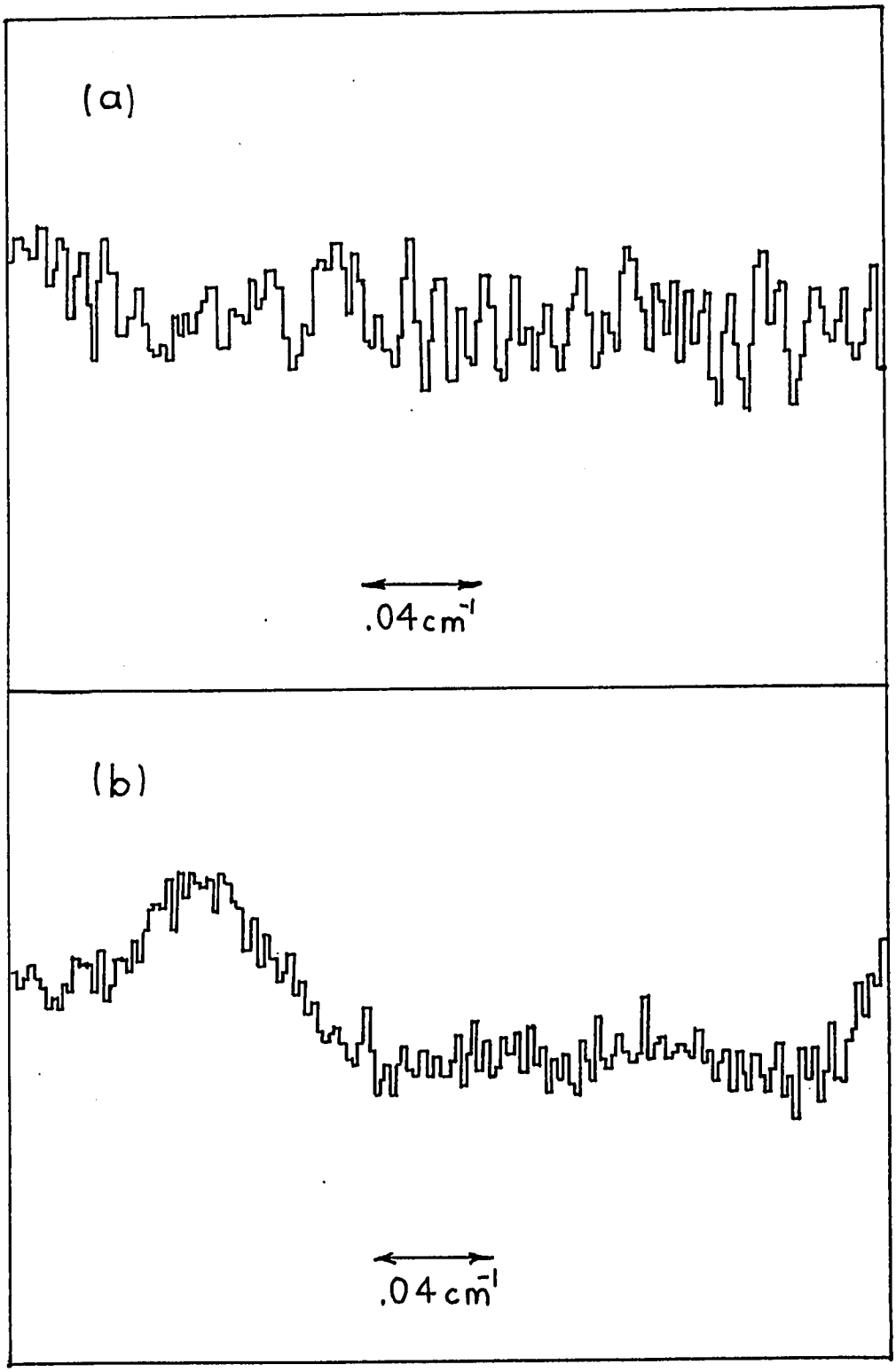
(a)
.04cm⁻¹
(b)
.04cm⁻¹

temperatures lower than 330°C, all the high resolution LIAF data showed no structure through the laser gain profile for the other lines.

B. Possible Mechanisms of LIAF Enhancement

1. Energy Transfer Effect

Baumgartner[37] claimed that the excited molecule can transfer energy to the ground state atom, by the reactions

$$Na_2 + h\nu \longrightarrow Na_2^*$$

$$Na_2^* + Na \longrightarrow Na_2 + Na^*$$

The excited atom then emits the atomic radiation. Since this is a nonresonant effect, the scattering cross section is small. We estimate the mean free path, $\ell = \frac{1}{n\sigma}$, to be in the order of 0.1 cm which is much larger than the laser beam diameter. In this estimation, we assumed the scattering cross section

$$\sigma = \frac{d^2}{v\ h} \simeq 10^{-14}\ cm^2$$

where v is molecular mean velocity and n is the molecular density. Thus the probability for energy transfer is very small.

2. Local Field Effect

Another possibility is the local field effect.[33] The LIAF signal depends on the local electric field which is the average of the external field plus the field from the induced dipole moment of the molecule. The local field, E_ℓ, is given

by

$$E_\ell = E_o + \frac{4\pi}{3} \frac{n\alpha}{(1 + \frac{4\pi}{3} n\alpha)} \cdot E_o$$

where E_o is the external laser field, n is the sodium molecular density and α is the total polarizability,

$$\alpha = \frac{e^2/m}{\omega^2 - \omega_o^2 + i\omega/\tau}$$

The magnitude of the polarizability at resonance is about 10^{-15} cm^{-3}, $|\alpha| = \frac{e^2\tau}{\omega m}$. At 300°C the dimer density is of the order of $10^{13}/cm^3$. Thus the correction for the local field, $n\alpha$, is very small ($n\alpha=10^{-2}$). In fact the density is the product of a Boltzman factor and the total density n, since only the dimers which are in resonance with laser should be counted. Thus the correction for local field becomes even smaller. So the external field can in effect be taken as the local field without modification.

3. Effects of the Highly Excited Atomic Sodium

If the high-lying states of the sodium atoms are excited, the atom will then decay to the ground state by emitting radiation, both on the D-line and on the highly excited atomic lines, thus artificially enhancing the LIAF signal.

We tested this effect by looking for the highly excited atomic lines. We set the cell temperature at 300°C and scanned through the positions of the highly excited lines (see Table 2). Even though some lines could have been obscured by molecular fluorescence, none could have represented more than 2% of the D-line intensity. We are thus confident that no such enhancement of our signal took place.

TABLE 2

The highly excited atomic states of sodium decay to the first excited states ($3P_{1/2}$, $3P_{3/2}$) with wavelength λ_1, λ_2 which are in the visible frequency range.

TABLE 2

Doubly Excited State	λ_1 (Å)	λ_2 (Å)
$5^2S_{1/2}$	6160.7	6154.3
$6^2S_{1/2}$	5153.6	5149.1
3^2D	8194.7	8183.3
4^2D	5688.2	5682.7
5^2D	4982.8	4978.6

4. Optical Pumping Effect

Since the LIAF signal is based on thermal distribution of the ground state, the optical pumping of the rotational-vibrational levels may be the most probable effect for this artificial enhancement. We discuss this in some detail in the following.

Laser irradiation excites a sodium molecule from the rotation-vibrational level of the ground state to the bound excited states in addition to the continuum states. The bound excited sodium molecule can then decay back to the rotation-vibrational levels of the ground state and enhance the population of particular levels. Thus the thermal distribution of the ground state, a basic assumption in our analysis of LIAF signal, can be modified.

The process of optical pumping is shown in Fig. 5. Laser irradiation induces a molecule from the rotation-vibrational level $|1\rangle$, of population n_1, to $|2\rangle$, of population n_2, at a rate $n_1 \varsigma B_{12}$ where ς is the energy density and B_{12} is the Einstein coefficient for induced transition. Laser irradiation also induces transition from $|2\rangle$ to $|1\rangle$ at rate $n_2 \varsigma B_{12}$. In addition, there is a spontaneous decay from $|2\rangle$ to $|k\rangle$ at a rate $n_2 A_{2k}$, where A_{2k} is the Einstein coefficient for spontaneous emission. At the same time, the laser field can perhaps induce a transition to higher order excited state $|M\rangle$ at a rate $n_2 \varsigma B_{2M}$, which is a higher order correction.

Since the lifetime[24], τ, of v'=10 state of $^1\pi_u$ is

Figure 5

Possible optical pumping routes in Na_2 which could result in spurious LIAF signals. The transition rates are determined by the Einstein A and B coefficients, including the Frank-Condon overlap factors between the various states, and the laser power density, ρ.

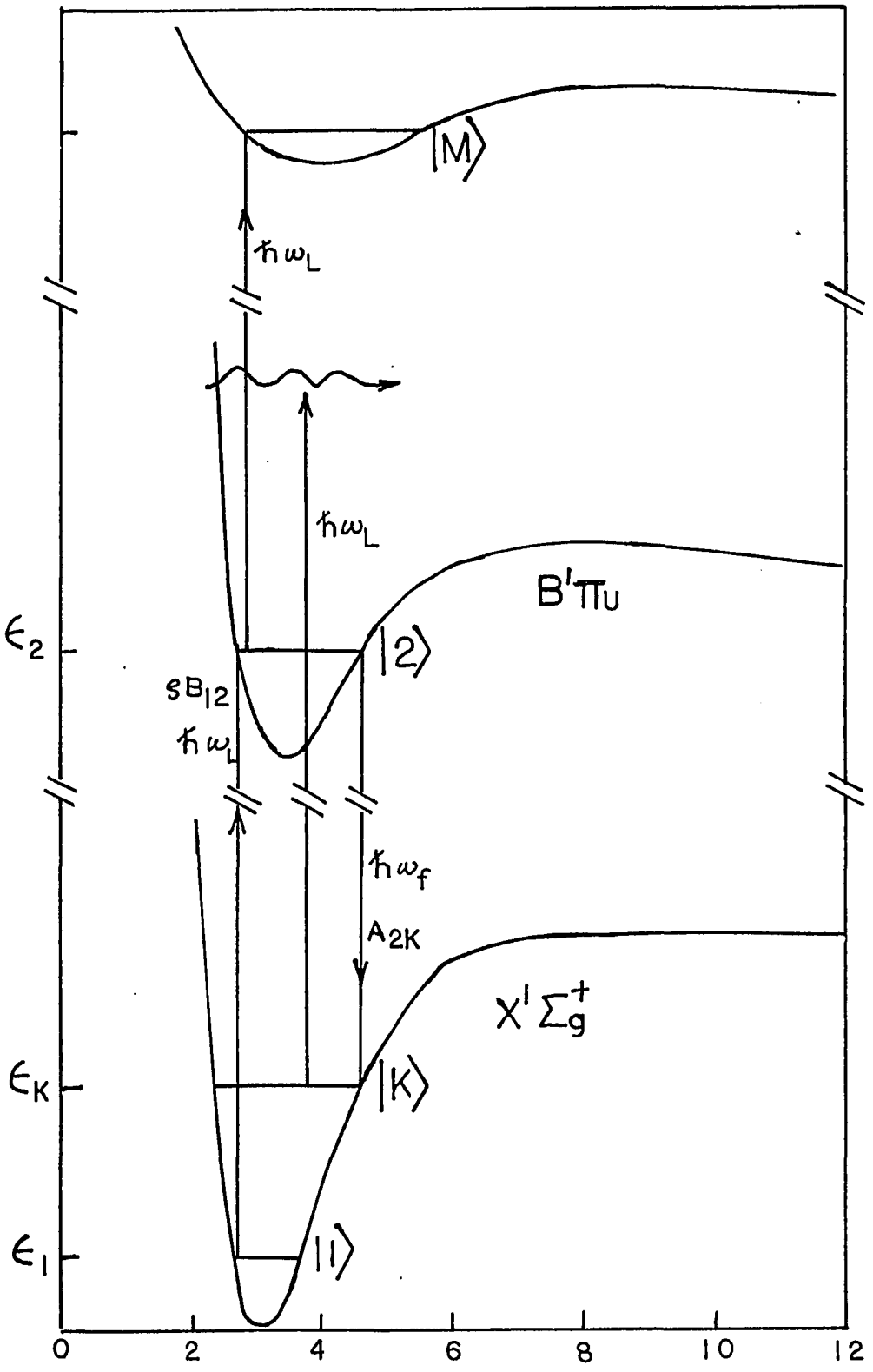
|M⟩
ħω_L
ħω_L
B'Πu
ε2
|2⟩
sB12
ħω_L
ħω_f
A2K
X'Σg+
εK
|K⟩
ε1
|1⟩
0
2
4
6
8
10
12

known to be 6.4nsec, the transition rate can be estimated. The spontaneous transition rate equals to $1/\tau$,

$$\frac{1}{\tau} = \sum_k A_2 |\langle 2 | k \rangle|^2 \simeq A_2$$

where $\langle 2|k\rangle$ is the Frank-Condon factor, and we assume a transition frequency of 19850 cm^{-1}, near the center of the π-Σ band system, rather than adjusting the transition probability by the 10% or so necessary to account for the variation in frequency across it. Since $B_{12} = A_{12}/8\pi hcv^3$

$$\rho B_{12} = 3.9 * 10^{10} |\langle 1 | 2 \rangle|^2 \left(\frac{2 S_{J1,J2}}{2J1+1} \right)$$

where $S_{J1,J2}$ is Honl-London[25] factor and ρ was taken to be 3.3 erg/cm^3-cm^{-1} corresponding to a laser spectral power density of 1 Watt-cm^{-1} focused into 10^{-4} cm^2. The rotational term, $\frac{2 S_{J1,J2}}{J1+1}$, is approximately equal to ½ (¼) for $\Delta J=0$ (± 1) transition for J=10; this is almost always the case.

At 300°C the thermal velocity is about $4*10^4$ cm/sec. Thus, after a molecule traveling in the beam for about $.1/|\langle 1|2\rangle|^2$ micron, the $|1\rangle$ and $|2\rangle$ levels, which are in resonance with laser, will be equally populated. The molecule in $|2\rangle$ can then decay to $|k\rangle$ with decay time being about $6.4/|\langle 2|k\rangle|^2$ nsec. A vibrational level where the absolute square of the Frank-Condon factor $|\langle 1|k\rangle|^2$ is of the order of .064 or greater will be enhanced in population. The LIAF signal will be distorted, if the enhanced level can

photodissociate.

In general, the optical pumping effect depends on the time a molecule spending in the beam, and the size of the resonance of the dimer transition in the well known $\Sigma_u - \Pi$ band. Thus the size of the laser beam where the signal was detected has to be narrowed down to reduce the time interval a molecule stays in the beam. For a typical transit time, a noticeable enhancement only occurs at some particular rotational-vibrational levels with large Frank-Condon factor.

At higher cell temperature (above 330°C), consequently higher sodium density, where the mean free path[26] of the sodium dimers, order of 1 cm at 330°C, becomes smaller than the cell dimension, the optical pumped (heated) dimers may not have a chance to relax back fully to thermal equilibrium before reentry into the laser beam, and this pumping mechanism will become more important. So by lowering the temperature this resonance pumping effect may be negligible. The high resolution experiments showed that at temperatures lower than 330°C the optical pumping can be neglected except 5017Å laser line. In this work we only consider the LIAF signal with a cell temperature lower than 330°C as being predicted by equation (4). And this experiment will be described in Chapter V.

CHAPTER V

EXPERIMENTAL DESIGN

A. Preliminary Experiment

The heat pipe oven was used in the earlier stage of LIAF experiment. The experimental setup was the same as described in Chapter IV (Fig. 3). In order to reduce the optical pumping effect as mentioned before, the temperature of the heat pipe oven (see Fig. 2) was controlled below 330°C. In fact, the temperature we operated was between 330°C and 290°C, since at lower temperatures (hence lower pressure) the heat pipe oven is not easy to control.

The multimode Ar^+ laser was used. The atomic fluorescence radiation was collected by scanning the Spex double monochrometer through the D-line wavelength, and the spectra was stored in the PDP-8 minicomputer.

Since the collecting lens was focused well within the sodium vapor (see Fig. 3), the D-lines appeared in self-reversal.[30] The detailed shape of self-reversed lines is strongly affected by the sodium density gradients present in our heat-pipe oven at the sodium-argon boundary. So we fitted only the wings of the self-reversed line, 10-50 cm^{-1} from the line center, where absorption is negligible. In this case, the signal is given by

$$\Gamma(\omega) = \Gamma_o\, g(\omega) \exp(-K g(\omega)) \simeq \Gamma_o\, g(\omega) \tag{16}$$

Here $g(\omega)$ is the resonance-broadened Lorentzian[31] profile evolving out of the actual Voight profile far from the line center at ω_o. The width of this Lorentzian,[32] δ, is proportional to the density, the optical-collision cross section, and the relative atomic velocities. Since the cross section is inversely proportional to the relative atomic velocity for resonance broadening based on dipole-dipole interactions, the width is then proportional only to n, the atomic density. The optical absorption depth is written as k in equation (16). Far from the center of the line, the Lorentzian[32] becomes $g(\omega) = \delta/(\omega - \omega_o)^2$. Equation (16) leads to

$$\Gamma(\omega) = \frac{\Gamma_o\, \delta}{(\omega - \omega_o)^2} \equiv \frac{A}{(\omega - \omega_o)^2} \tag{17}$$

The variable, A, was then obtained by a least squares fit of equation (17) to the wings of the D-line (16978 cm^{-1}). Since two D lines are separated by 18 cm^{-1} the contribution from wing of 16960 cm^{-1} line to $\Gamma(\omega)$, equation (17), is less than 10%.

For a complete set of LIAF measurements, we held the temperature and pressure constant and measured the D-line signal using the different argon laser lines. For a fixed

temperature (hence fixed density) the width, δ , which is proportional to n, becomes a constant over a set of LIAF measurements. Thus the resulting variable A can be considered as the LIAF signal apart from a constant factor. The typical D-line intensity versus the internuclear separation which is in resonance with the laser is plotted in Fig. 6.

The self-reversal problem made the deduction of D-line intensity difficult. The optical-absorption depth, k,one of the factors that control self-reversal, is not easy to adjust since Ar-Na boundary is not well defined at this temperature range. Also, low density, i.e. low temperature, so as to minimize k, is difficult to reach. Thus we changed the sodium container from the heat pipe oven to the glass cell and redesigned the experimental setup described below. In this new arrangement, the right angle scattered geometry took the place of the back scattered. As it is possible to focus the laser beam close to the window, the self absorption of the D-line signal will be reduced more than three times.

B. Equipment

The sodium vapor container consisted of two parts: the cell and reservoir. The cell, where the laser beam passed through, was made of alkali-resistant Corning 1720 alumino-silicate glass. The reservoir, containing sodium metal, is made of pyrex. Both of them were placed in an oven consisting of an aluminum block with heaters in it, surrounded by insulating fire brick. There were two thermocouples inside the oven in contact with the glass. One

Figure 6

Typical data for $\Gamma_o\delta$ as a function of the internuclear separation at 300°C temperature of the heat pipe oven.

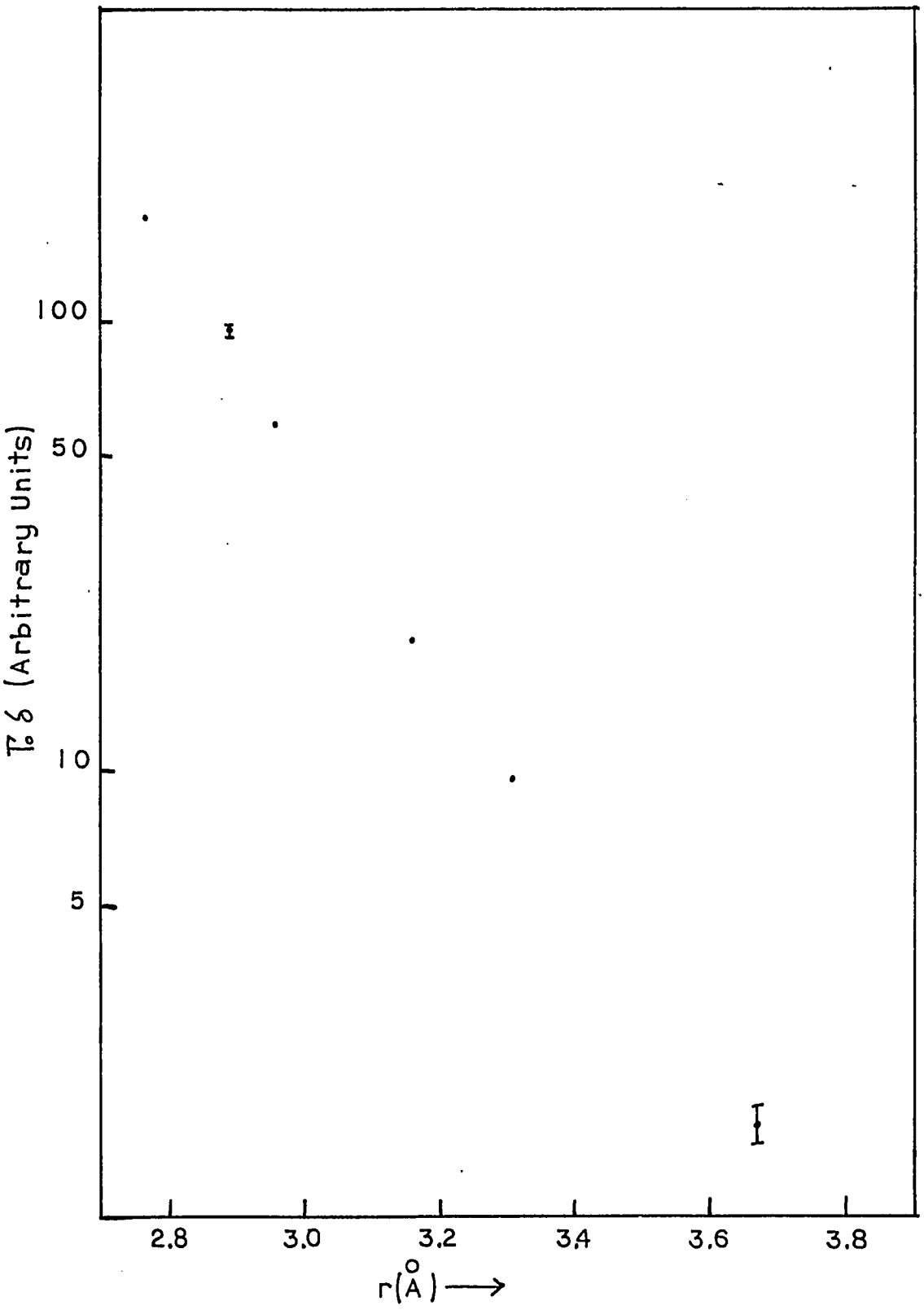
100
50
10
5
T₀δ (Arbitrary Units)
2.8
3.0
3.2
3.4
3.6
3.8
r(Å) ⟶

measured the cell temperature using ice water as a standard. This thermocouple was also connected to a Leeds and Northrup temperature controller (series 80), which can adjust the output of the power supply to the heater directly and maintain the cell temperature at a preset temperature within .25°C. Another thermocouple measured the temperature difference between the cell and the reservoir, where the reservoir temperature is about 5°C lower than that of the cell.

A schematic drawing of the complete apparatus is shown in Fig. 7. A Spectra-Physics model 165 Ar^+ laser and a Coherent Radiation model 52B Kr^+ laser were used. As stated before, the laser beam must be focused to a very narrow beam inside the Na-cell. The telescope, made of the two lenses L_1 and L_2, magnifies the diameter of the laser by a factor of three. Another lens, L_3, with focal length = 25 cm, then focuses this beam into the cell. By assuming the diffraction at a circular aperature, the focal region[34] is limited by $\Delta d = 1.2\ (f/d)\lambda$ in diameter and $\Delta z = 2.4\ (f/d)^2\lambda$ along the optical axis. So the laser beam inside the cell was narrowed to about 40 micron in diameter over a distance of about 6 mm. L_1, L_2 and L_3 were achromatic lenses to minimize the longitudinal change in the location of the focal point as the incident laser frequency varied. Lense L_4 magnifies the D-line signal and images it into the .25 mm X 2.cm slit of the .25 meter spectrometer (Spex Minimate, model 1670). To minimize the

Figure 7

The experimental arrangement showing the laser, lens arrangement, sodium cell, collection optics, and detection equipment as described in the text. The laser intensity was also measured both before and after the cell to normalize the D-line intensity.

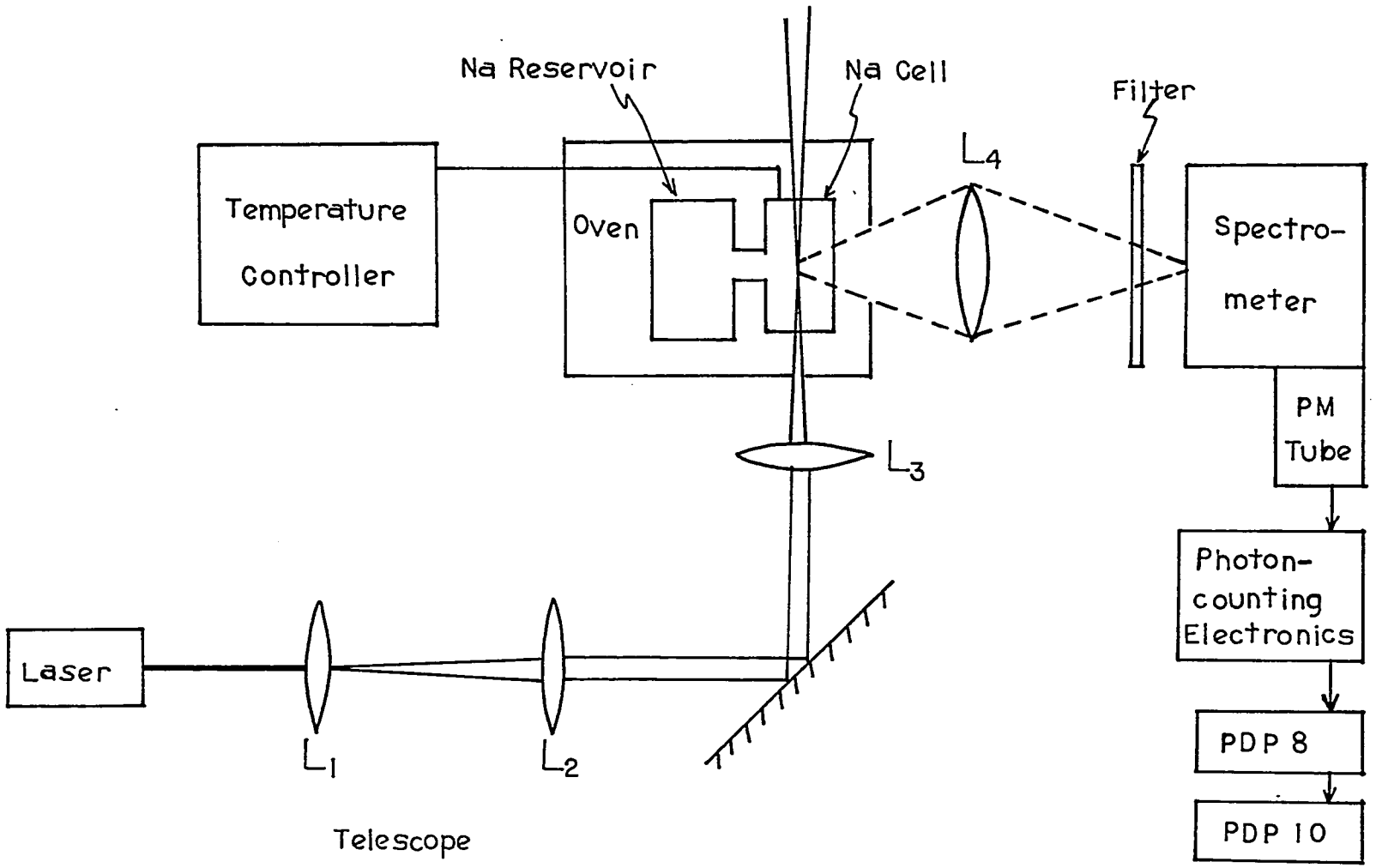
Na Reservoir
Na Cell
Filter
Temperature Controller
Oven
L_4
Spectro-meter
PM Tube
L_3
Photon-counting Electronics
Laser
L_1
L_2
PDP 8
PDP 10
Telescope

amount of the scattered light from the cell, a broad band interference filter centered on the D-line wavelength was placed in front of the slit. The spectrometer scanned through the D-line wavelength (5800 Å - 6000 Å), and the LIAF signal was detected by a cooled EMI 9558 photomultiplier tube. The resulting spectra, detected by a standard photon counting electronic which was interfaced to a PDP-8e minicomputer, were stored and transferred to a PDP-10 computer for further analysis as described below.

Significant deterioration of the sample cell occurred after a few hours of use due to a glass-sodium reaction which changed the glass spectral transmission function. Thus with the laser intensity before entering the cell I_i and that after leaving the cell I_o, we use the value $\sqrt{I_o I_i}$ to normalize the D-line emission signal for both varying input intensity as well as the glass spectral transmission from line to line. The cell spectral transmission at the D-line wavelength was measured before and after the experiment and no changes were found during the measurement time.

C. Date Collection and Reduction

After the temperature was stabilized, we started the data collection process. When the spectrometer passed through a preset wavelength (5800 Å), the computer received a signal and began storing the data. The temperature of the cell was set between 210°C and 270°C (220, 225, 230, 240, 250 and 260°C). At the high end of this range, all seven Ar^+ laser lines (4658, 4727, 4765, 4880, 4965, 5145, and 5287 Å)

and four Kr^+ lines (4762, 4825, 5208 and 5309 Å) were used. At lower temperature ranges only the five strongest Ar^+ lines could be used due to the smaller sodium density and, hence, smaller LIAF signal. Fig. 8 shows the LIAF signal plotted against the internuclear separation for two temperatures. For each point, the radius corresponds to that at which the laser frequency is in resonance with the separation of the ground and excited state potential curves; these radii are listed in Table 1.

The D-line intensity was determined from the observed spectrum at a given exciting wavelength and temperature after correction for the spectral transmission function of the spectrometer plus interference filter. We found that the transmission function of the interference filter was well fitted to the empirical formula

$$f(\lambda) = \Delta^b/(\Delta^b + |\lambda - \lambda_0|^b)$$

with $\Delta = 46$ Å, $b = 2.3$ and $\lambda_0 = 5867$ Å. The transmission function of the spectrometer, $f_s(\lambda, \lambda_s)$, with variable wavelength λ when spectrometer set at λ_s, was well given by a triangular shape

$$f_s(\lambda, \lambda_s) = \begin{cases} \dfrac{s - |\lambda - \lambda_s|/D}{s}, & \text{for } \lambda_s - sD \le \lambda \le \lambda_s + sD, \\ 0, & \text{otherwise}, \end{cases} \tag{18}$$

Figure 8

The LIAF signal as a function of internuclear separation for two cell temperatures, 220°C and 270°C.

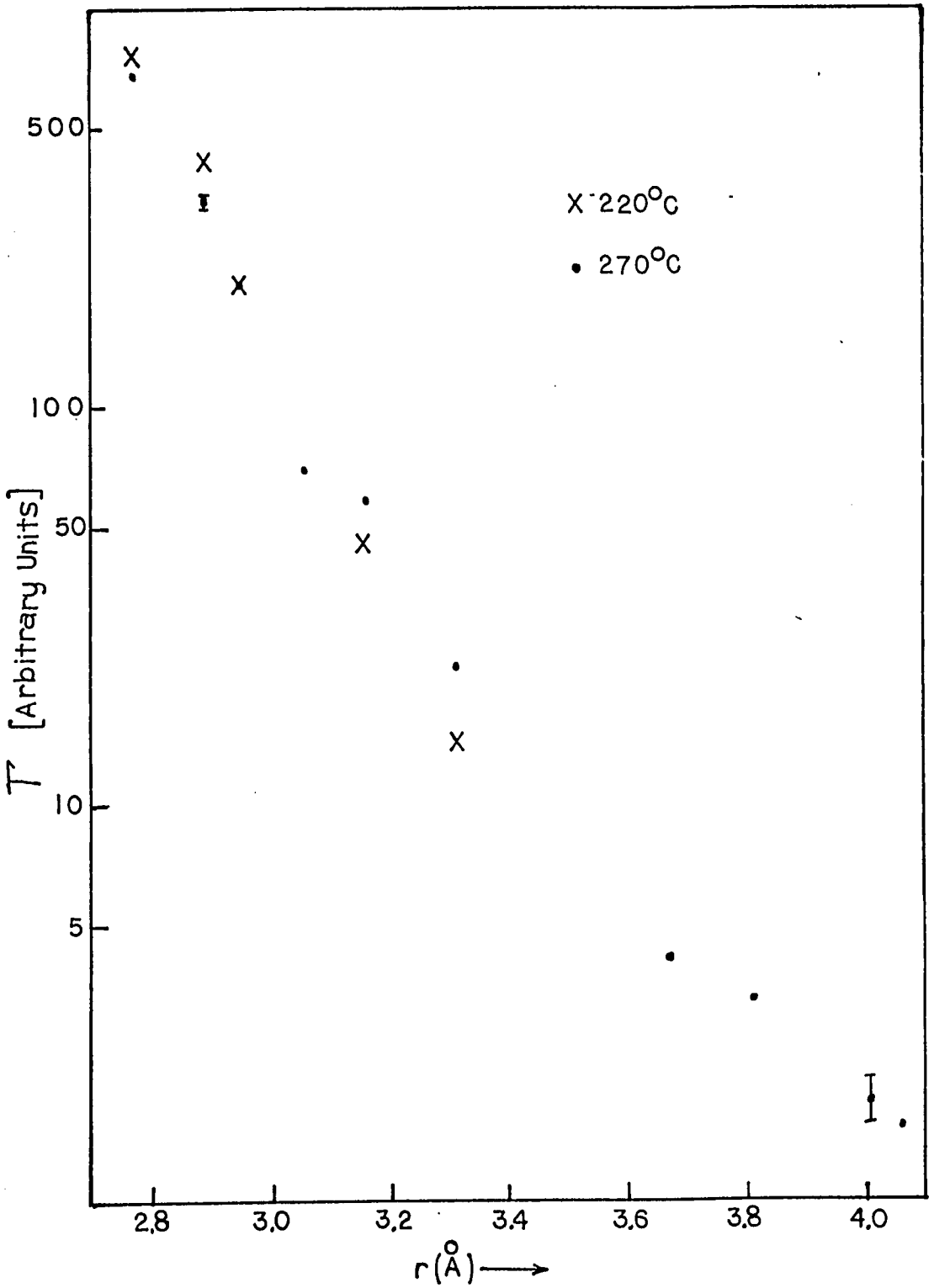
500
100
50
10
5
T [Arbitrary Units]
X 220°C
• 270°C
2.8
3.0
3.2
3.4
3.6
3.8
4.0
r(Å) ⟶

where s, the slit width, is .25 mm and D, the dispersion of the grating, is 40 Å/mm. Thus the total transmission function is given by

$$F(\lambda, \lambda_s) = f_s(\lambda, \lambda_s) * f(\lambda)$$

Taking the D-line to be the delta functions with integrated intensity Γ at $\lambda_1 = 5889.95$ Å for the $3^2P_{3/2}$ state, and $\frac{1}{2}\Gamma$ at $\lambda_2 = 5895.9$ Å for the $3^2P_{\frac{1}{2}}$ state, and assuming a constant background intensity I_b, the intensity at λ_s, $I(\lambda_s)$ will be given by

$$I(\lambda_s) = \int d\lambda\, F(\lambda,\lambda_s) \left[\Gamma\, \delta(\lambda-\lambda_1) + \frac{1}{2}\Gamma\, \delta(\lambda-\lambda_2) + I_b \right] + I_d \qquad (19)$$

where I_d is the known dark current of the PM tube. Γ and I_b are then determined by a least squares fit to the observed LIAF spectral profile, $I(\lambda_s)$. The dark current and background signals combined typically amounted to less than 10% of the total signal.

The next step is to reduce the dissociation energy and the transition moment from the data set. Equation (4) shows that $\Gamma(\omega_i, T_j)$, the magnitude of D-line intensity, depends on the laser frequency ω_i, density, and temperature T_j. At the same temperature, the geometry of the setup for different laser frequencies is the same. In order to avoid complications due to the inaccuracy in determining the sodium density and the D-line self-absorption problem, the

measured intensities at each temperature T_j were normalized to one standard intensity, $\mathcal{P}(\omega_s, T_j)$. By Equation (4), the intensity ratio at the same temperature T_j, is

$$\frac{\mathcal{P}(\omega_i, T_j)}{\mathcal{P}(\omega_s, T_j)} = \frac{M^2(r_i)}{M^2(r_s)} \frac{G(r_i, D')}{G(r_s, D')} e^{-\beta_j(\epsilon_1(r_i) - \epsilon_1(r_s))} \cdot \left(\frac{r_i}{r_s}\right)^2 \frac{\left| d(\epsilon_2 - \epsilon_1)/dr \right|_{r_s}}{\left| d(\epsilon_2 - \epsilon_1)/dr \right|_{r_i}}$$

$$= \frac{M^2(r_i)}{M^2(r_s)} f_{ij}(D') \qquad (20)$$

where $M(r_i)/M(r_s)$ is the ratio of the transition moment at the internuclear separation r_i, to that at r_s. The function, $f_{ij}(D')$, depends on the dissociation energy D' (see Fig. 1), on the different laser frequencies, ω_i, ω_s, and temperature T_j as well.

The relative transition moments and the dissociation energy could then be determined by least squares fitting equation (20) to the measured D-line intensities for different temperature and laser frequencies.

CHAPTER VI

RESULTS AND DISCUSSION

A. Dissociation Energy

From our measurement, the dissociation energy D', of the excited electronic $^1\pi_u$ state was found to be 3300 ± 200 cm^{-1} (All of our error estimates represent one standard deviation, derived from the statistical properties of the data and the quality of the fit.) This value agrees satisfactorily with the result of Hessel and Kusch,[18] 3110 cm^{-1}, and that of Demtroder and Stock,[19] 3090 ± 50 cm^{-1}. Both of these two values were obtained from analysis of the molecular fluorescence lines of the sodium dimers.

B. Variation of the Transition Moment

The results of the transition rate versus the internuclear separation is shown in Fig. 9; the large error bars at large r is due to the poor photon counting statistics resulting from small signals in this region. Since our method does not give the magnitude of the transition moment, the value calculated from the lifetime data of Demtroder and Zare was used as a standard. The lifetime of $v' = 10$ level of B $^1\pi_u$ state,[24] with which 4765 Å laser line resonates, is 6.41 ± .38 nsec. With the value of Frank-Condon factors[18] in

Figure 9

The transition moment as a function of internuclear separation obtained from the LIAF signal using equation 4. Also shown are the experimental results of Hessel et al.[35] and the theoretical predictions of Tango and Zare[36] for comparison purposes. The left hand ordinate in the transition moment normalized to that at λ_L = 4765 Å (r = 2.959 Å); the right hand ordinate is the absolute transition moment normalized to give 8.11 Debye at 2.96 Å (see text).

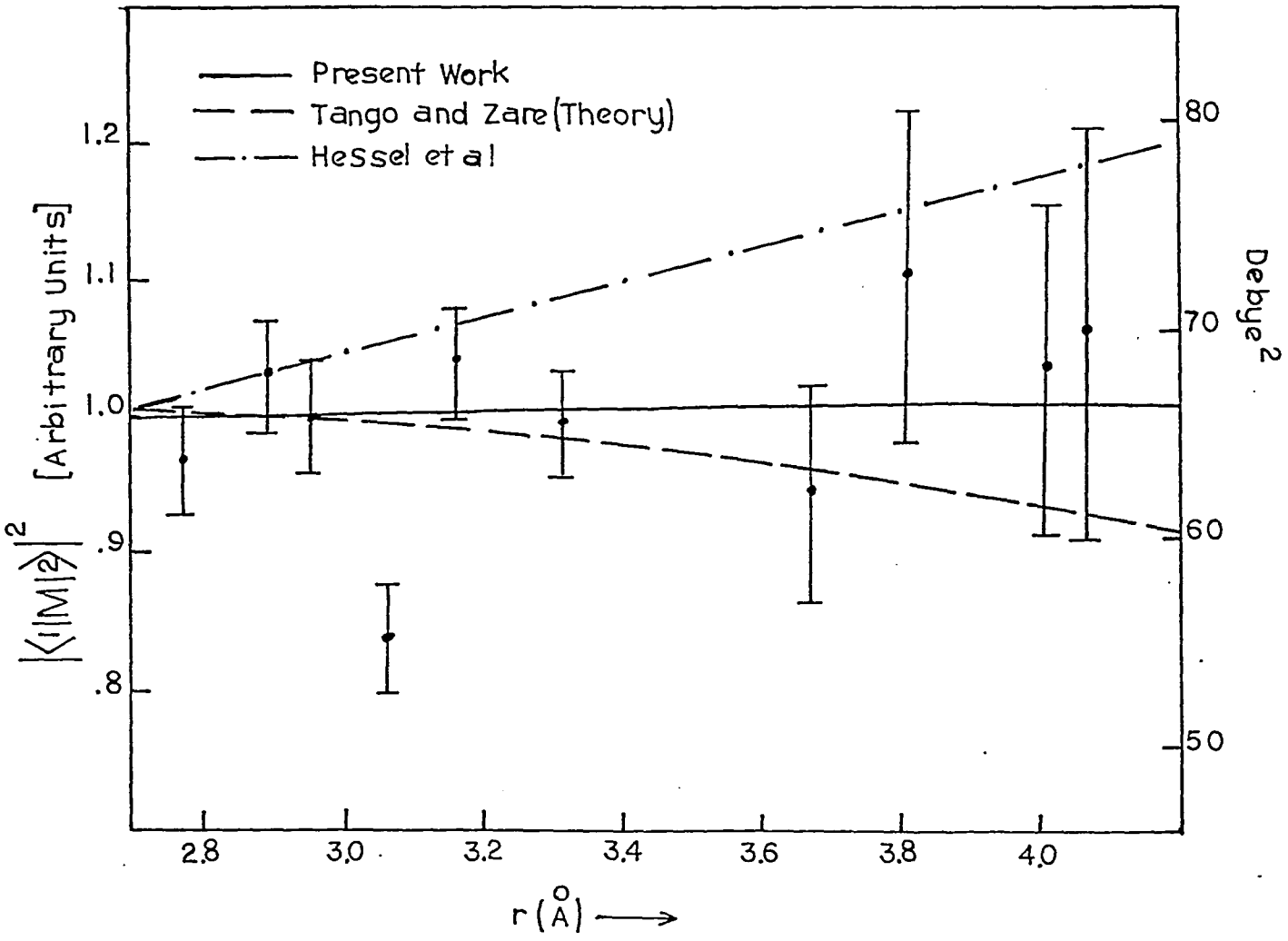
Present Work
Tango and Zare (Theory)
Hessel et al
1.2
1.1
1.0
.9
.8
$|\langle 1|M|2\rangle|^2$ [Arbitrary Units]
80
70
60
50
Debye^2
2.8
3.0
3.2
3.4
3.6
3.8
4.0
r (Å) ⟶

$$\frac{1}{\tau} = \frac{64\pi^4}{3h} \bar{R}e^2 \sum_{v''} \nu_{v'v''}^3 \langle v' | v'' \rangle^2$$

it was found that the average transition moment, $\bar{R}e$ = 8.11 Debye at r = 2.96 Å, where the molecule is in resonance with the 4765 Å laser line (see Table 1). Our results have thus been scaled so that the relative transition moment is 8.11 Debye at 2.96 Å. A least squares fit the data to a linear function, $M(r) = M_o + ar$, using the inverse of the variance as the weighting factors resulted in M_o = 8.1 ± .8 Debye and a=.01 ± .25 Debye/Å.

Fig. 9 also shows the experimental results of Hessel[35] et al. for transition moment and the theoretical calculation of Tango and Zare.[36] Hessel's results were determined from the intensities of the molecular fluorescence series, ((v' = 10, J' = 12) → (v", J" = 11 and 13) and (v' = 6, J' = 43) → (v", J" = 43)), which were excited by 4765 Å and 4880 Å laser lines. Following the conventional method, they obtained the transition moment, $M(r) = M_o + ar$, with M_o = 6.8 Debye and a = .5 ± .2 Debye/Å. Our results and theirs agree to within experimental errors. Tango and Zare's calculation is based on the simple Coulomb wave function with the effective quantum number n* = 2, since the calculation using n* = 2.1, the effective quantum number for sodium[42] would only change the radial scaling and reduce the r → 0 and r → ∞ asymptotes slightly.[35] The results agree well with the LIAF data on the transition moment although it is only a

simple model.

In reference (35), Hessel et al. also reduced the data of Baumgartner et al. on the lifetimes of various excited vibrational states of Na_2 to obtain $M_o = 6.8 \pm 0.2$ D and $a = 0.4 \pm 0.1$ D/Å. However, these results are suspectable due to a questionable procedure used in the work of Baumgartner et al. They obtained the lifetimes of the individual vibrational levels of $^1\pi_u$ by measuring the phase shift between a rapidly modulated laser beam and the modulations in the resulting molecular fluorescence. However, they did not shield against D-line radiation, which, since the atomic excited state has a much longer lifetime, would make the molecular lifetimes appear longer in proportion to the amount of atomic radiation present. They ascribed the D line radiation to collisional energy transfer and assumed that its effect would be negligible if they extrapolated their measured lifetimes to zero pressure. Our experiments show that this is not the case, and that in fact, the zero-collision D line intensity will increase with laser frequency by a factor of 10 over the range of laser frequencies they used, and could quite possibly account for the increase in lifetimes they measured with those various laser frequencies. It is possible that the self-absorption of the D lines lengthened the effective lifetime of the ^2P state of Na so much that the D line fluorescence was not modulated. So we would not regard these results as a verification.

Williams and Rousseau[38] had re-analyzed our earlier

published data using a fully quantum mechanical approach. Using the Born-Oppenheimer approximation, they started from equation (9) and calculated the atomic fluorescence intensity by numerically integrating Schrodinger's equation for the vibrational wave function. The results show constant transition moment from 2.9 Å to 3.7 Å, which agrees well with our measurement. This agrees with our WKB results that quantum mechanical effect is unimportant in the analysis as described before. However, in the range between 2.7 Å and 2.9 Å, their calculation shows a variation of the transition moment decreasing linearly which is different from our results. It is also in disagreement with theoretical calculations and with the experimental results of the others. Their calculation was based on the older RKR potentials[39] which did not cover the potential energy of B $^1\pi_u$ excited state at the nuclear separation smaller than 2.84 Å and did not include potential barrier on the B $^1\pi_u$ state. Thus, the increase in the transition moment for small r probably represents an artificial enhancement produced by inaccuracies in the old potentials.

The results of the transition moment between B $^1\pi_u$ and X $^1\Sigma_g^+$ states of Na_2 is nearly constant in the range of 2.7 Å and 4.1 Å. These results show that Condon principle is approximately valid over the region of our measurement. However, the transition moment as function of nuclear separation is expected to vary over the entire range of the internuclear separation out to the free-atom limit, since

the lifetime of the dimer is usually different from the lifetime of the free atom. In the case of sodium, the lifetime of the dimer in B $^1\pi_u$ state is approximately a factor of three shorter than the free atom's lifetime.[31] Thus, by a suitable choice of a series of laser frequencies, we should be able to see the variation of the transition moment as a function of the internuclear separation.

C. Scattering Cross Section

Since LIAF is a resonance phenomenon, a large scattering cross section is expected. We can estimate the total cross section, σ_t, which is defined as the ratio of the number of photons scattered per unit time per molecule to the incident laser flux.

At 200°C, using 4880 Å as the exciting laser irradiation with a flux of $1.5*10^{22}$ photons/cm^2-sec, equivalent to 80 mW laser power with 40 μ diameter, we obtained the scattered D-line signal of 660 photons/sec. The efficiencies of the detectors can be estimated as that of the PM tube = 0.08, minimate spectrometer = 0.15, the transmission of the sodium cell and the interference filter = 0.25. Further, with 50% of self-absorption of the D-line signal, solid angle = 0.4 at a sodium dimer density of $3*10^{10}$, we found $\sigma_t = 1.0*10^{-20}$ cm^2. Equation (4) predicts a total cross section of $\sigma_t = 2.6*10^{-19}$ cm^2 under the same conditions where the transition moment is taken to be 8.0 Debye. The agreement between experimental and theoretical results is reasonably good.

CHAPTER VII

CONCLUSION

We wish to emphasize that the LIAF technique for measuring the spectroscopic properties of molecular systems, e.g., the transition moment for different internuclear separations and aspects of the potential curves, is quite simple and useful. Since the intensity at only one atomic fluorescence frequency is measured, there is no need of calibration of the precise spectral response of the spectrometer and photomultiplier tube. Also, by using a semi-classical approximation in the analysis, the results are easy to obtain and to understand. For instance, in order to find the variation of the transition moments, we need only a least squares fit of a straightforward algebraic formula to the LIAF data. And to obtain the dissociation energy of the excited state, we need only one more parameter in the least squares fit, while the standard treatments require Birge-Sponer extrapolations[40] based on the analysis of large number of spectral lines.

Besides finding the variation of the transition moment and dissociation energy of sodium molecule, the LIAF technique and semi-classical approximation which describes it can easily be applied to other molecular systems, e.g., K_2, I_2 as well as polyatomic molecules. This technique can also be

used in the reverse sense as used here. That is, the potential curve[9] of a molecule can be measured if the excited state is unbound.

REFERENCES

[1]R. H. Callender, J. I. Gersten, R. W. Leigh and J. L. Yang, Phys. Rev. Lett. 32 917 (1974).

[2]R. H. Callender, J. I. Gersten, R. W. Leigh and J. L. Yang, Phys. Rev. Lett. 33 1311 (1974).

[3]P. A. Fraser, Can. J. Phys. 32 515 (1954)

[4]J. J. Sakurai, Advanced Quantum Mechanics (New York: Addison-Wesley, 1967).

[5]H. Goldstein, Classical Mechanics (New York: Addison-Wesley, 1950), Chapter 3.

[6]Abramowitz and Segun, Handbook of Mathematical Functions (New York: Dover, 1968).

[7]G. Hertzberg, Spectra of Diatomic Molecules (New York: Van Nostrand Reinhold Co., 1950), pp. 425 ff.

[8]G. W. King and J. H. Van Vleck, Phys. Rev. 55 1165 (1939).

[9]J. I. Gersten, Phys. Rev. Lett. 31 73 (1973).

[10]A. S. Davydov, Quantum Mechanics (New York: Pergamon Press, 1965), Chapter III.

[11]Wavelengths in Air taken from W. B. Bridges and A. N. Chester,"Ionized Gas Lasers" in the C.R.C. Handbook of Lasers, R. J. Pressley, ed. (Cleveland: Chem. Rubber Co., 1972). Reduced to vacuum using a formula for (n-1) from The American Institute of Physics Handbook, D. E. Grey, ed. (New York: McGraw Hill, 1972), p. 611.

[12]M. Lax, Phys. Rev. 20 1752 (1952).

[13]P. Morse and H. Feshbach, Method of Theoretical Physics (New York: McGraw Hill, 1953), pp. 240 and 414.

[14]W. H. Louisell, Radiation and Noise in Quantum Electronics (New York: McGraw Hill, 1964), Chapter 3.

[15]F. B. Hildebrand, Introduction to Numerical Analysis (New York: McGraw Hill, 1956), pp. 49-50.

[16]R. H. Margenau and N. R. Kentner, Theory of Intermolecular Forces (New York: Pergamon Press, 1969).

[17]L. I. Schiff, Quantum Mechanics (New York: McGraw-Hill, 1968).

[18]P. Kusch and M. M. Hessel, unpublished work.

[19]W. Demtroder and M. Stock, J. Mol. Spec. 55 476 (1975).

[20]Handbook of Chemistry and Physics, D. D. Hodgeman, ed. 42nd p. 2921.

[21]R. S. Mulliken, Phys. Rev. 120 1674 (1960).

[22]G. Stephenson, Proc. Phys. Soc. London A64 458 (1951).

[23]M. Sargent, M. Scully and W. E. Lamb Jr., Laser Physics (New York: Addison Wesley, 1974), Ch. II.

[24]M. McClintock, W. Demtroder and R. N. Zare, J. Chem. Phys. 51 5509 (1969).

[25]Reference 7, p. 208.

[26]Chapman, S., Kinetic Theory of Glass in Fundamental Formulas of Physics, D. H. Menzel, ed. (New York: Dover, 1960).

[27]C. R. Vidal and J. Cooper, J. Appl. Phys. 40 3370 (1969).

[28] Floyd Todd, Ind. Eng. Chem. Anal. 20 1248 (1948).

[29]A. N. Nesmeyanov, Vapor Pressure of the Chemical Elements (New York: Elsevier, 1963).

[30]R. D. Cowan and G. H. Dieke, Rev. Mod. Phys. 20 418 (1948).

[31]A. C. Mitchell and M. W. Zemansky, Resonance Radiation and Excited Atoms (Cambridge, England: Cambridge Univ. Press, 1961).

[32]R. G. Breene, The Shift and Shape of the Spectral Lines (New York: Pergamon Press, 1961).

[33]M. V. Klein, Optics (New York: John Wiley & Sons, Inc., 1970).

[34]M. Born and E. Wolf, Principles of Optics (New York: Pergamon Press, 1970).

[35]M. M. Hessel, E. W. Smith and R. E. Drullinger, Phys. Rev. Lett. 33 1251 (1974).

[36]W. Tango and R. N. Zare, J. Chem. Phys. 53 3094 (1970)

[37]F. Baumgartner, W. Demtroder and M. Stock, Z. Physik 232 462 (1970).

[38]P. F. Williams and D. C. Rousseau, Phys. Rev. Lett. 33 1516 (1974).

[39]W. Demtroder, M. McClintock and R. N. Zare, J. Chem. Phys. 51 5495 (1969).

[40]Reference 7, pp. 437 ff.